PHYSICAL REVIEW B VOLUME 2, NUMBER 10 15 NOVEMBER 1970

Crystal-Field Effects in the Tight-Binding Approximation: ReO_3 and Perovskite Structures

L. F. Mattheiss
Bell Telephone Laboratories, Murray Hill, New Jersey 07974
(Received 22 April 1970)

The augmented-plane-wave (APW) band structure of ReO_3 is analyzed in terms of the Slater-Koster linear-combination-of-atomic-orbitals (LCAO) interpolation scheme with nonorthogonal orbitals. This approach has several advantages over an earlier treatment involving orthonormal basis functions. First, it provides insight into the physical origin of the crystal-field splittings in ReO_3 and other transition-metal compounds. Second, it leads to more physically meaningful LCAO parameters. Finally, it provides a direct relationship between the crystal-field levels of an isolated transition-metal ion or molecular complex and the band structure of the periodic crystal. In the case of ReO_3, it is shown that the crystal-field effects are due to overlap and covalency between the rhenium $5d$ orbitals and the $2s$, $2p\sigma$, and $2p\pi$ orbitals of the neighboring oxygen ligands. The splitting between the e_g and t_{2g} bands is due to the $2s$ contribution Δ_s. The difference between the $2s$ and $2p\sigma$ contributions $\Delta_\sigma - \Delta_s$ is responsible for the e_g bandwidth. This same difference is proportional to the effective transfer integral b in Anderson's theory of superexchange. The t_{2g} bandwidth is due to Δ_π, the $2p\pi$ overlap-covalency parameter. This LCAO method is applied to $KNiF_3$, using LCAO integrals determined from the Sugano-Shulman molecular-orbital calculation for the $(NiF_6)^{4-}$ complex. The resulting $KNiF_3$ band structure is qualitatively similar to the APW results for ReO_3, except the bandwidths are narrower by about a factor of 4. In the limit where the Coulomb energy U is large compared with the e_g and t_{2g} bandwidths so that the electrons localize, it is shown that the crystal-field splitting between the localized e_g and t_{2g} Wannier functions is identical with that obtained by Sugano and Shulman via the molecular-orbital method.

I. INTRODUCTION

In a previous study of the band structure and Fermi surface of ReO_3 by the author[1] (hereafter referred to as I), the linear-combination-of-atomic-orbitals (LCAO) interpolation scheme of Slater and Koster[2] was applied to interpolate between the results of augmented-plane-wave (APW) calculations at symmetry points in the Brillouin zone. The resulting Fermi surface was found to be in quantitative agreement with experiment. The calculated cross-sectional areas agreed to within 10% with the de Haas–van Alphen data of Marcus.[3] The maximum discrepancy between the calculated and experimental Fermi-surface areas was reduced to about 5% when a comparison was made with the more accurate magnetothermal oscillation data of Graebner and Greiner.[4]

Despite this excellent agreement between theory and experiment concerning the dimensions and shape of the ReO_3 Fermi surface, it was recognized that this LCAO parameterization scheme included the crystal-field splitting between the rhenium t_{2g} ($5d$ orbitals of xy, yz, and zx symmetry) and e_g (those of $3z^2-r^2$ and x^2-y^2 symmetry) states in a rather artificial way. Namely, this splitting was introduced into the LCAO scheme by shifting the orbital energy of the e_g states relative to that of the t_{2g} orbitals by the crystal-field splitting Δ. As a result, all the crystal-field effects exhibited by the APW results for ReO_3 were buried in a single one-center d-type LCAO parameter, namely, $E_{3z^2-r^2,3z^2-r^2}(000)$ in the notation of Slater and Koster.[2]

The present analysis represents an attempt to provide a more physical representation of these crystal-field effects in the ReO_3 and closely related perovskite band structures. To do this, we introduce one of the complications that Slater and Koster removed at the outset in their treatment of the LCAO interpolation scheme. Namely, we form our Bloch sums from nonorthogonal atomiclike orbitals rather than the orthogonalized combinations suggested by Slater and Koster. After the secular equation for a given wave vector $\vec{k}$ has been set up in terms of these nonorthogonal Bloch sums, we then apply the symmetrical orthogonization method of Löwdin[5] to convert to an orthonormal basis. In the nonorthogonal basis, all the d orbitals have approximately the same energy and the final crystal-field splittings between the e_g and t_{2g} levels are the result of overlap and covalency between the oxygen $2s$-$2p$ and the rhenium e_g orbitals.

The details of the generalized LCAO interpolation scheme for ReO_3 involving nonorthogonal atomic orbitals are presented in Sec. II. Section III contains a detailed analysis of the crystal-field splittings of some particularly simple states at symmetry points of the simple cubic Brillouin zone for the ReO_3 structure. It is shown that the crystal-field splitting at Γ, for example, is due entirely to

oxygen 2s and rhenium e_g overlap and covalency effects. The resulting shift in the e_g orbital energy is denoted by Δ_s. On the other hand, at the point R, similar but stronger interactions between the oxygen $2p\sigma$ and rhenium e_g orbitals produce a larger shift Δ_σ. At other symmetry and nonsymmetry points in the Brillouin zone, the crystal-field splittings contain a combination of these effects.

Section IV contains a second-order perturbation-theory treatment of these effects. To this approximation, it is shown that the difference $\Delta_\sigma - \Delta_s$ has the same wave-vector dependence as the LCAO d-d parameter which is responsible for the e_g bandwidth. It is also shown that the analogous overlap-covalency interactions between the oxygen $2p\pi$ and rhenium t_{2g} orbitals lead to a similar parameter Δ_π, which is largely responsible for the t_{2g} bandwidth.

In Sec. V we establish a relationship between the present tight-binding approach and the molecular-orbital (MO) method used by Sugano and Shulman (SS)[6] in their treatment of the $(NiF_6)^{4-}$ complex in $KNiF_3$. Using their variational method, but imposing the translational symmetry of the lattice, we find detailed expressions for covalency and crystal-field parameters which are equivalent to the results of Secs. III and IV. We examine these results in the limit where the Coulomb interaction energy U between two d orbitals on the same atom is large compared to the e_g and t_{2g} bandwidths, thereby causing the Bloch waves to localize into Wannier functions whose energy is the *average* energy of the corresponding band states. It is shown that the crystal-field splitting between the localized e_g and t_{2g} states is given by the simple expression

$$\Delta_{1oc} = E_{d\sigma} - E_{d\pi} + \tfrac{1}{2}(\Delta_s + \Delta_\sigma - \Delta_\pi), \tag{1.1}$$

where $E_{d\sigma}$ and $E_{d\pi}$ correspond to the energies of the nonorthogonal e_g and t_{2g} orbitals. To second order in perturbation theory, Δ_{1oc} is identical with the expression for the crystal-field parameter Δ that is obtained by Sugano and Shulman via the MO method.

The results that are obtained from applying the LCAO method with nonorthogonal orbitals to ReO_3 and $KNiF_3$ are contained in Sec. VI. These results include energy bands, LCAO wave functions, and an evaluation of the accuracy of second-order perturbation theory. Section VII contains a summary of this approach to crystal-field theory and its relationship to earlier methods. It includes some comments concerning the extension of these methods to other crystal structures and the implications of these results on Anderson's theory of superexchange.[7]

II. LCAO METHOD: NONORTHOGONAL ORBITALS

In the present application of the Slater-Koster LCAO method, we form Bloch sums from atomic orbitals which are not orthogonal to each other. As Slater and Koster point out, this procedure yields nonorthogonal Bloch functions. However, we shall show that this lack of orthogonality does not represent a serious handicap to the LCAO method in actual numerical computations. Furthermore, it is believed that this procedure provides a more physical representation of both the energy bands $E(\vec{k})$ and the corresponding Bloch-type wave functions $b_n(\vec{k})$.

The original treatment of ReO_3 in I with orthogonal orbitals $\psi_n(\vec{r})$ included the oxygen $2p$ orbitals of x, y and z symmetry localized at each of the three oxygen sites in the unit cell. Five additional Bloch functions were formed from the rhenium $5d$ orbitals of xy, yz, zx, $3z^2$-r^2, and x^2-y^2 symmetry. In the present treatment, we include these same basis functions, except they are now formed from nonorthogonal orbitals $\varphi_n(\vec{r})$. In addition, we augment this basis set by including oxygen 2s orbitals at each of the three oxygen sites. This increases the dimension of the secular equation from 14 to 17. In principle, we could also include the rhenium 6s orbitals in this scheme, but the APW results in I indicate that the bands formed from these states lie above the rhenium $5d$ bands, well above the ReO_3 Fermi energy. We will return to this point in later sections.

In order to simplify the analysis, we shall include only the largest overlap effects. These occur between the rhenium e_g and the oxygen 2s and $2p\sigma$ orbitals. This is clear from the schematic representation of these orbitals in Fig. 1. The two-center integral involving φ_s and $\varphi_{3z^2-r^2}$ of Fig. 1(a) and the Hamiltonian operator is denoted by $(sd\sigma)$. The corresponding overlap integral is represented by S_s. Similarly, the corresponding energy and overlap integrals involving φ_z and $\varphi_{3z^2-r^2}$ in Fig.

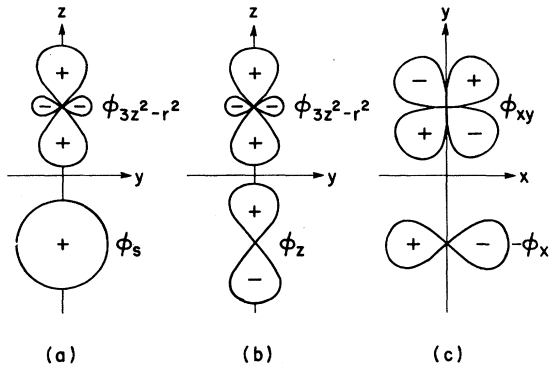

FIG. 1. (a) Schematic representation of a single σ bond involving rhenium $\varphi_{3z^2-r^2}$ and oxygen φ_s orbitals. (b) Orbitals involved in a single σ-type bond. (c) Orbitals which form a π-type bond.

TABLE I. Additional nonvanishing LCAO matrix elements for the ReO_3 structure which augment Table III (I) by including overlap and s-d interactions.

Tight-binding basis functions			
	No.	Origin	Function
Oxygen s	15	$\frac{1}{2}a(1,0,0)$	s_1
	16	$\frac{1}{2}a(0,1,0)$	s_2
	17	$\frac{1}{2}a(0,0,1)$	s_3

Oxygen-oxygen (s-s) interactions

$$E_s \equiv E_{s_1, s_1}(000)$$

$$H_{15,15} = H_{16,16} = H_{17,17} = E_s$$

Oxygen-rhenium (p-d) overlap

$$S_\sigma \equiv S_{z3,3z^2-r^2}(00\tfrac{1}{2})$$

$$S_{6,4} = -iS_\sigma \sin\tfrac{1}{2}\xi \qquad S_{6,5} = \sqrt{3}\, iS_\sigma \sin\tfrac{1}{2}\xi$$
$$S_{10,4} = -iS_\sigma \sin\tfrac{1}{2}\eta \qquad S_{10,5} = -\sqrt{3} iS_\sigma \sin\tfrac{1}{2}\eta$$
$$S_{14,4} = 2iS_\sigma \sin\tfrac{1}{2}\zeta$$

Oxygen-rhenium (s-d) interactions

$$(sd\sigma) \equiv E_{s3,3z^2-r^2}(00\tfrac{1}{2})$$

$$H_{15,4} = -(sd\sigma)\cos\tfrac{1}{2}\xi \qquad H_{15,5} = \sqrt{3}\,(sd\sigma)\cos\tfrac{1}{2}\xi$$
$$H_{16,4} = -(sd\sigma)\cos\tfrac{1}{2}\eta \qquad H_{16,5} = -\sqrt{3}\,(sd\sigma)\cos\tfrac{1}{2}\eta$$
$$H_{17,4} = 2(sd\sigma)\cos\tfrac{1}{2}\zeta$$

Oxygen-rhenium (s-d) overlap

$$S_s \equiv S_{s3,3z^2-r^2}(00\tfrac{1}{2})$$

$$S_{15,4} = -S_s \cos\tfrac{1}{2}\xi \qquad S_{15,5} = \sqrt{3}\, S_s \cos\tfrac{1}{2}\xi$$
$$S_{16,4} = -S_s \cos\tfrac{1}{2}\eta \qquad S_{16,5} = -\sqrt{3}\, S_s \cos\tfrac{1}{2}\eta$$
$$S_{17,4} = 2S_s \cos\tfrac{1}{2}\zeta$$

1(b) are denoted by $(pd\sigma)$ and S_σ, respectively. Finally, the energy integral involving the orbitals φ_{xy} and φ_x in Fig. 1(c) is represented by $(pd\pi)$ and the corresponding overlap integral S_π is neglected in the present simplified analysis. (We shall include these π overlap terms later in the $KNiF_3$ calculation.)

The detailed form of the LCAO matrix that was applied in the earlier treatment of ReO_3 is contained in Table III of I [hereafter referred to as Table III (I)]. The additional energy and overlap integrals which enter the present treatment are contained in Table I. The notation for the overlap integrals is derived by analogy with the Slater-Koster notation for the energy integrals with S replacing E.

Once the Hamiltonian and overlap matrices have been set up for a particular wave vector $\vec{k}$, we can immediately apply the Löwdin symmetric orthogonalization scheme[5] to convert back to an orthonormal basis. As Slater and Koster prove, this transformation preserves the point-group symmetry of the φ_n orbitals in the orthonormal basis. If $\underline{H}$ is the Hamiltonian matrix in the nonorthogonal basis with overlap matrix $\underline{S}$, then Löwdin's symmetric orthogonalization scheme introduces an effective Hamiltonian matrix $\underline{H}'$ with a unit overlap matrix, where

$$\underline{H}' = \underline{S}^{-1/2}\, \underline{H}\, \underline{S}^{-1/2} \ , \tag{2.1}$$

and $\underline{S}^{-1/2}$ is a symmetric, nonunitary matrix that satisfies the relation

$$\underline{S}^{-1/2}\, \underline{S}\, \underline{S}^{-1/2} = \underline{1} \ . \tag{2.2}$$

Löwdin has given a power-series expansion of $\underline{S}^{-1/2}$.[5] However, when the overlap is large, the convergence of this power-series expansion is quite slow and it is necessary to determine $\underline{S}^{-1/2}$ more directly for numerical computations. A method for determining $\underline{S}^{-1/2}$ that is convenient for machine calculations involves the following procedure[8]: The $\underline{S}$ matrix is first diagonalized by a unitary transformation $\underline{U}$ to yield the diagonal matrix $\underline{d}$,

$$\underline{U}^\dagger\, \underline{S}\, \underline{U} = \underline{d}. \tag{2.3}$$

Since the eigenvalues of $\underline{S}$ are all positive, a new matrix $\underline{d}^{-1/2}$ can be formed from $\underline{d}$ by replacing each diagonal element by its inverse square root. Then, the matrix $\underline{S}^{-1/2}$ is given by

$$\underline{S}^{-1/2} = \underline{U}\, \underline{d}^{-1/2}\, \underline{U}^\dagger \ . \tag{2.4}$$

The matrix $\underline{S}^{-1/2}$ is clearly self-adjoint and is easily shown to satisfy Eq. (2.2).

III. CRYSTAL-FIELD SPLITTING: Γ_{12}, X_2, M_2, AND R_{12}

It is instructive to consider in some detail a simple example of these effects in the ReO_3 structure and show how covalency and overlap each contribute to the crystal-field splitting. By introducing a slightly generalized notation, we can consider several important examples at once, namely, the states with Γ_{12}-, X_2-, M_2-, and R_{12}-type symmetry.[1] The importance of these states is immediately clear from the results of Table I (I). There, it is shown that states with Γ_{12} and X_2 symmetry occur in the rhenium $5d$ and oxygen $2s$ bands but not the oxygen $2p$ band. On the other hand, M_2 and R_{12} states occur only in the rhenium $5d$ and oxygen $2p\sigma$ bands. These states are simpler than those with X_1- or M_1-type symmetry since the former interact either with oxygen $2s$ or $2p\sigma$ orbitals but not both. Thus, we can separate out rather easily the relative contributions to the crystal-field splitting that result from $2s$-$5d$ and $2p\sigma$-$5d$ covalency and overlap effects.

To proceed, we apply the appropriate unitary transformations to the LCAO Hamiltonian and overlap matrices of Table I and Table III (I). The reduced matrices for Γ_{12}, X_2, M_2, and R_{12} each have the form

$$\underline{H} = \begin{pmatrix} E_\alpha & \sqrt{6}\,(\alpha d\sigma) \\ \sqrt{6}\,(\alpha d\sigma) & E_d \end{pmatrix} \ , \tag{3.1a}$$

$$\underline{S} = \begin{pmatrix} 1 & \sqrt{6}\, S_\alpha \\ \sqrt{6}\, S_\alpha & 1 \end{pmatrix} \ , \tag{3.1b}$$

where $\alpha = s$ or p; S_p is equivalent to S_σ of Table I, and we use the two-center notation to replace the LCAO parameter P_2 of Table III (I) by $(pd\sigma)$. To simplify this discussion, we have ignored temporarily the small nearest-neighbor p-p and d-d interaction terms that contribute to the diagonal in Eq. (3.1a) and have included only the one-center integrals, which we denote by E_s, E_p, and E_d. Additional subscripts σ and π will be added later to E_p and E_d, but they are omitted now to simplify the notation. In terms of the integrals defined in Table III (I), $E_{p\sigma} = A_1$, $E_{p\pi} = B_1$, $E_{d\sigma} = D_4$, $E_{d\pi} = D_1$. The omitted p-p and d-d interactions will be replaced later in the detailed application to ReO_3 that is described in Sec. VI A.

Using the results of Sec. II, the matrix $\underline{S}^{-1/2}$ is readily determined. Its matrix elements are given by

$$(S^{-1/2})_{11} = (S^{-1/2})_{22} = \tfrac{1}{2}[(1+\sqrt{6}\,S_\alpha)^{-1/2} + (1-\sqrt{6}\,S_\alpha)^{-1/2}],$$
$$(S^{-1/2})_{21} = (S^{-1/2})_{12} = \tfrac{1}{2}[(1+\sqrt{6}\,S_\alpha)^{-1/2} - (1-\sqrt{6}\,S_\alpha)^{-1/2}]. \tag{3.2}$$

Using this result, we can determine the effective Hamiltonian $\underline{H}'$ of Eq. (2.1). These matrix elements are given by

$$\begin{aligned}(H')_{11} &= [2(1-6S_\alpha^2)]^{-1}\{[1+(1-6S_\alpha^2)^{1/2}]E_\alpha \\ &\quad + [1-(1-6S_\alpha^2)^{1/2}]E_d - 12S_\alpha(\alpha d\sigma)\},\\ (H')_{12} &= (H')_{21} = [2(1-6S_\alpha^2)]^{-1} \\ &\quad \times [-\sqrt{6}\,S_\alpha(E_\alpha+E_d) + 2\sqrt{6}\,(\alpha d\sigma)],\\ (H')_{22} &= [2(1-6S_\alpha^2)]^{-1}\{[1-(1-6S_\alpha^2)^{1/2}]E_\alpha \\ &\quad + [1+(1-6S_\alpha^2)^{1/2}]E_d - 12S_\alpha(\alpha d\sigma)\}.\end{aligned} \tag{3.3}$$

These expressions can be simplified if the two-center integral $(\alpha d\sigma)$ is separated into two terms. This integral involves the Hamiltonian operator H_{op} and the orbitals φ_α and $\varphi_{3z^2-r^2}$. As is usual in band theory, H_{op} is a sum of the kinetic energy T and potential terms V_α and V_d, so that

$$H_{op} = T + V_\alpha + V_d, \tag{3.4}$$

which can be rewritten

$$H_{op} = \tfrac{1}{2}(T+V_\alpha) + \tfrac{1}{2}(T+V_d) + \tfrac{1}{2}(V_\alpha+V_d). \tag{3.5}$$

Here, V_α and V_d are the atomiclike potentials of the oxygen and rhenium atoms, respectively. Then

$$\begin{aligned}(\alpha d\sigma) &\equiv \int \varphi_\alpha(\vec{r}) H_{op} \varphi_{3z^2-r^2}(\vec{r} - \tfrac{1}{2}a\vec{k})\,dv \\ &= \tfrac{1}{2}S_\alpha(E_\alpha+E_d) + V_{\alpha d},\end{aligned} \tag{3.6}$$

where $V_{\alpha d}$ results from the third term on the right-hand side in Eq. (3.5). Using this result in Eq. (3.3) and combining terms, we are led to a simplified form for $\underline{H}'$:

$$(H')_{11} = E_\alpha - \tfrac{1}{2}[(1-6S_\alpha^2)^{-1/2} - 1](E_d - E_\alpha) - 6S_\alpha V_{\alpha d}(1-6S_\alpha^2)^{-1}, \tag{3.7a}$$

$$(H')_{21} = (H')_{12} = \sqrt{6}\,V_{\alpha d}(1-6S_\alpha^2)^{-1}, \tag{3.7b}$$

$$(H')_{22} = E_d + \tfrac{1}{2}[(1-6S_\alpha^2)^{-1/2} - 1](E_d - E_\alpha) - 6S_\alpha V_{\alpha d}(1-6S_\alpha^2)^{-1}. \tag{3.7c}$$

Let us consider some of the features of H' that follow from Eq. (3.7). First, we observe that H' reduces to H when the overlap integral S_α goes to zero since the second and third terms in $(H')_{11}$ and $(H')_{22}$ vanish, and $(\alpha d\sigma)$ is then equal to $V_{\alpha d}$ according to Eq. (3.6). If we apply the diagonal sum rule to $(H')_{11}$ and $(H')_{22}$, we find that the second terms cancel and we have

$$(H')_{11} + (H')_{22} = E_\alpha + E_d - 12S_\alpha V_{\alpha d}(1-6S_\alpha^2)^{-1}. \tag{3.8}$$

The first two terms on the right-hand side of Eq. (3.8) are just the diagonal sum of $\underline{H}$ according to Eq. (3.1a). Thus, the center of gravity of the orthogonalized states is raised relative to that of the nonorthogonal orbitals by the last term on the right-hand side in Eq. (3.8). We define this term B_α as

$$B_\alpha \equiv -12S_\alpha V_{\alpha d}(1-6S_\alpha^2)^{-1}. \tag{3.9}$$

If we choose the phase of the wave functions $\varphi_n(\vec{r})$ so that the overlap integral S_α is positive, then it is clear from Eqs. (3.5) and (3.6) that $V_{\alpha d}$ is negative and B_α is positive. In any case, S_α and $V_{\alpha d}$ will always have opposite signs so B_α will always be positive. If we also define

$$A_\alpha \equiv \tfrac{1}{2}[(1-6S_\alpha^2)^{-1/2} - 1](E_d - E_\alpha), \tag{3.10}$$

then by substituting Eqs. (3.9) and (3.10) into Eq. (3.7), we find

$$(H')_{11} = E_\alpha - A_\alpha + \tfrac{1}{2}B_\alpha, \tag{3.11a}$$

$$(H')_{12} = (H')_{21} = \tfrac{1}{2}B_\alpha/\sqrt{6}\,S_\alpha, \tag{3.11b}$$

$$(H')_{22} = E_d + A_\alpha + \tfrac{1}{2}B_\alpha. \tag{3.11c}$$

Since the oxygen $2s$ and $2p$ bands are located below the rhenium $5d$ bands, $E_d > E_s$ and E_p so that A_α is also positive.

The implications of Eq. (3.11) are illustrated schematically in Fig. 2. To the left we show the orbital energies E_d and E_α. Moving to the right, we first add the terms A_α and then $\frac{1}{2}B_\alpha$, both of which occur on the diagonal of $(H')_{11}$ and $(H')_{22}$ in Eq. (3.11). The sum of these terms corresponds to the diagonal energies of the orthogonalized orbitals E'_α and E'_d, respectively. Finally, the effect

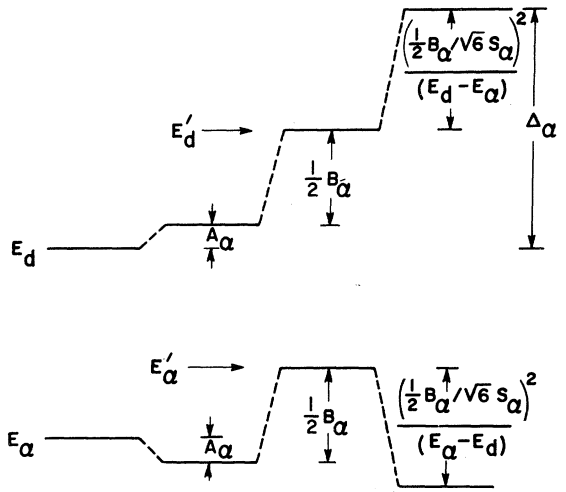

FIG. 2. Schematic representation of the relative magnitudes of the various terms in Eq. (3.11), as described in the text.

of the off-diagonal matrix element $(H')_{12}$ is included (to second order in perturbation theory) to obtain the final states shown to the far right. The total energy shift of the d orbitals is indicated by Δ_α.

To determine Δ_α, we solve the secular equation that results from $\underline{H}'$ of Eq. (3.11). To second order the energies of the bonding and antibonding states (E_α^b and E_α^a) are given by

$$E_\alpha^b = E_\alpha - A_\alpha + \tfrac{1}{2}B_\alpha - \frac{(\frac{1}{2}B_\alpha/\sqrt{6}\,S_\alpha)^2}{(E_d - E_\alpha + 2A_\alpha)} + \cdots , \quad (3.12)$$

$$E_\alpha^a = E_d + A_\alpha + \tfrac{1}{2}B_\alpha + \frac{(\frac{1}{2}B_\alpha/\sqrt{6}\,S_\alpha)^2}{(E_d - E_\alpha + 2A_\alpha)} - \cdots . \quad (3.13)$$

We define the total energy shift of the d orbital by the parameter Δ_α, where

$$\Delta_\alpha \equiv E_\alpha^a - E_d , \quad (3.14)$$

so that

$$\Delta_\alpha = A_\alpha + \tfrac{1}{2}B_\alpha + \frac{(\frac{1}{2}B_\alpha/\sqrt{6}\,S_\alpha)^2}{(E_d - E_\alpha + 2A_\alpha)} - \cdots . \quad (3.15)$$

If A_α and B_α are expanded in powers of $\sqrt{6}\,S_\alpha$ and $\sqrt{6}\,V_{\alpha d}$, keeping only second-order terms, we find

$$A_\alpha \approx \tfrac{1}{4}(\sqrt{6}\,S_\alpha)^2(E_d - E_\alpha) , \quad (3.16)$$

$$B_\alpha \approx -2(\sqrt{6}\,S_\alpha)(\sqrt{6}\,V_{\alpha d}). \quad (3.17)$$

Substituting these results into Eq. (3.15), dropping the $2A_\alpha$ in the denominator of the third term on the right-hand side, and simplifying, we find the following expression for Δ_α:

$$\Delta_\alpha \approx [\tfrac{1}{2}\sqrt{6}\,S_\alpha(E_d - E_\alpha) - \sqrt{6}\,V_{\alpha d}]^2/(E_d - E_\alpha). \quad (3.18)$$

Using Eq. (3.6), an equivalent expression for Δ_α is given by

$$\Delta_\alpha \approx [-\sqrt{6}\,(\alpha d\sigma) + \sqrt{6}\,S_\alpha E_d]^2/(E_d - E_\alpha). \quad (3.19)$$

By proceeding in a similar manner, we can determine the analogous contribution to the energy of the α orbital that is due to the formation of a partially covalent bond:

$$E_\alpha^b - E_\alpha \approx -[\tfrac{1}{2}\sqrt{6}\,S_\alpha(E_d - E_\alpha) + \sqrt{6}\,V_{\alpha d}]^2/(E_d - E_\alpha). \quad (3.20)$$

The terms within the brackets of the numerator add in Eq. (3.18) and cancel in Eq. (3.20). Thus, to second order, the d-orbital shift Δ_α is energetically greater than the covalent bonding effect in the valence bands.

IV. PERTURBATION-THEORY TREATMENT

In contrast to the detailed analysis of the crystal-field effects involving particular states at symmetry points in the Brillouin zone, we now present a more general treatment of these effects using second-order perturbation theory. For this analysis, a matrix formulation of perturbation theory due to Löwdin[9] is particularly convenient. For simplicity, we include explicitly for the moment only the d orbitals with e_g symmetry in this analysis. The wave equation for the nonorthogonal oxygen $2s$, $2p$, and rhenium e_g orbitals $\varphi_n(\vec{r})$ can be written in the matrix form

$$\begin{pmatrix} \underline{H}_{ss} & 0 & \underline{H}_{sd} \\ 0 & \underline{H}_{pp} & \underline{H}_{pd} \\ \underline{H}_{sd}^\dagger & \underline{H}_{pd}^\dagger & \underline{H}_{dd} \end{pmatrix} \begin{pmatrix} \vec{C}_s \\ \vec{C}_p \\ \vec{C}_d \end{pmatrix} =$$

$$\begin{pmatrix} E\underline{1} & 0 & E\underline{S}_{sd} \\ 0 & E\underline{1} & E\underline{S}_{pd} \\ E\underline{S}_{sd}^\dagger & E\underline{S}_{pd}^\dagger & E\underline{1} \end{pmatrix} \begin{pmatrix} \vec{C}_s \\ \vec{C}_p \\ \vec{C}_d \end{pmatrix} , \quad (4.1)$$

where the eigenvector $\vec{C}$ has been decomposed into s, p, and d components, as indicated by the subscripts. If Eq. (4.1) is multiplied out, $\vec{C}_s$ and $\vec{C}_p$ can be eliminated, and Eq. (4.1) can be replaced by a single equation involving an effective Hamiltonian $\underline{H}'_{dd}$ and $\vec{C}_d$:

$$\underline{H}'_{dd}\vec{C}_d = E\vec{C}_d , \quad (4.2)$$

where

$$\underline{H}'_{dd} = \underline{H}_{dd} + (\underline{H}_{sd}^\dagger - E\underline{S}_{sd}^\dagger)\,(E\underline{1} - \underline{H}_{ss})^{-1}\,(\underline{H}_{sd} - E\underline{S}_{sd}) + (\underline{H}_{pd}^\dagger - E\underline{S}_{pd}^\dagger)\,(E\underline{1} - \underline{H}_{pp})^{-1}\,(\underline{H}_{pd} - E\underline{S}_{pd}) . \quad (4.3)$$

If we define

$$\Delta_{dd}^\alpha \equiv (\underline{H}_{\alpha d}^\dagger - E\underline{S}_{\alpha d}^\dagger)\,(E\underline{1} - \underline{H}_{\alpha\alpha})^{-1}\,(\underline{H}_{\alpha d} - E\underline{S}_{\alpha d}) , \quad (4.4)$$

then

$$\underline{H}'_{dd} = \underline{H}_{dd} + \underline{\Delta}_{dd}^s + \underline{\Delta}_{dd}^p . \quad (4.5)$$

At this point, the analysis is still exact. We now introduce the approximations which reduce this treatment to that of second-order perturbation theory. If we retain only the diagonal terms in the expansion of $(E\underline{1}-\underline{H}_{\alpha\alpha})^{-1}$, set $E=E_d$, and $\underline{H}_{\alpha\alpha}=E_\alpha\underline{1}$ in Eq. (4.4), we then find the following form for $\underline{\Delta}^s_{dd}$ and $\underline{\Delta}^p_{dd}$ in the case of the ReO_3 structure:

$$
\begin{aligned}
&(\Delta^s_{dd})_{44}=\tfrac{1}{6}\Delta_s(\cos^2\tfrac{1}{2}\xi+\cos^2\tfrac{1}{2}\eta+4\cos^2\tfrac{1}{2}\zeta)\,,\\
&(\Delta^s_{dd})_{45}=(\Delta^s_{dd})_{54}=\sqrt{3}\,\tfrac{1}{6}\Delta_s(-\cos^2\tfrac{1}{2}\xi+\cos^2\tfrac{1}{2}\eta)\,,\\
&(\Delta^s_{dd})_{55}=\tfrac{1}{2}\Delta_s(\cos^2\tfrac{1}{2}\xi+\cos^2\tfrac{1}{2}\eta);
\end{aligned}
\tag{4.6}
$$

$$
\begin{aligned}
&(\Delta^p_{dd})_{44}=\tfrac{1}{6}\Delta_p(\sin^2\tfrac{1}{2}\xi+\sin^2\tfrac{1}{2}\eta+4\sin^2\tfrac{1}{2}\zeta)\,,\\
&(\Delta^p_{dd})_{45}=(\Delta^p_{dd})_{54}=\sqrt{3}\,\tfrac{1}{6}\Delta_p(-\sin^2\tfrac{1}{2}\xi+\sin^2\tfrac{1}{2}\eta)\,,\\
&(\Delta^p_{dd})_{55}=\tfrac{1}{2}\Delta_p(\sin^2\tfrac{1}{2}\xi+\sin^2\tfrac{1}{2}\eta)\,.
\end{aligned}
\tag{4.7}
$$

Here, the indices 4 and 5 refer to the e_g orbitals $3z^2-r^2$ and x^2-y^2, respectively, following the notation of Table III (I). The parameter Δ_α is given by Eq. (3.18) with α equal to s or p.

Equations (4.6) and (4.7) contain the contributions of the oxygen $2s$ and $2p\sigma$ orbitals to the crystal-field parameter. In Sec. VI, we shall show that Δ_p is two or three times larger than Δ_s. If we write

$$\Delta_s+6D_\Delta=\Delta_p\,, \tag{4.8}$$

then $6D_\Delta$ turns out to be a positive quantity that is largely responsible for the e_g bandwidth. Assuming for the moment that D_Δ is negligible, then Eq. (4.5) simplifies to

$$\underline{H}'_{dd}=H_{dd}+\Delta_s\underline{1}\,, \tag{4.9}$$

since the $\sin^2\frac{1}{2}x$ and $\cos^2\frac{1}{2}x$ terms in Eqs. (4.6) and (4.7) add up to one and the off-diagonal contributions cancel. Thus, according to Eq. (4.9), the energy of the e_g orbitals is increased relative to that of the t_{2g} states by the crystal-field parameter Δ_s.

We now consider the effect of the $6D_\Delta$ term in Eq. (4.8). This adds a wave-vector–dependent term $\underline{H}^{\vec{k}}_{dd}$ to the right-hand side of Eq. (4.9), where

$$
\begin{aligned}
&(H^{\vec{k}}_{dd})_{44}=3D_\Delta-2D_\Delta(\tfrac{1}{4}\cos\xi+\tfrac{1}{4}\cos\eta+\cos\zeta)\,,\\
&(H^{\vec{k}}_{dd})_{45}=(H^{\vec{k}}_{dd})_{54}=-\tfrac{1}{2}\sqrt{3}\,D_\Delta(-\cos\xi+\cos\eta)\,,\\
&(H^{\vec{k}}_{dd})_{55}=3D_\Delta-\tfrac{3}{2}D_\Delta(\cos\xi+\cos\eta)\,.
\end{aligned}
\tag{4.10}
$$

Comparing with the results of Table III (I), it is clear that $\underline{H}^{\vec{k}}_{dd}$ has the same cosine-dependent terms as

$$D_5\equiv E_{3z^2-r^2,\,3z^2-r^2}(001)\,.$$

Therefore, we can introduce an effective parameter D'_5 which includes to second order the direct d-d interaction D_5 plus the anisotropic crystal-field parameter D_Δ,

$$D'_5=D_5-D_\Delta\,. \tag{4.11}$$

These two contributions to D'_5 add rather than cancel since D_5 is negative according to the results of Table V(I) and D_Δ is positive. Neglecting D_6 [which is small according to the results of Table V(I)], the e_g bandwidth is $-6D'_5$. The total e_g bandwidth in ReO_3 therefore includes a small contribution from direct d-d interactions; the major contribution is due to the anisotropic component of the crystal field D_Δ.

An analogous treatment of the t_{2g} and $2p\pi$ orbitals is straightforward. The s-d interactions vanish by symmetry. For these t_{2g} states, $\underline{H}'_{dd}$ contains the additional $2p\pi$ interaction terms $\underline{H}^{\vec{k}}_{dd}$, where

$$
\begin{aligned}
&(H^{\vec{k}}_{dd})_{11}=\tfrac{1}{2}\Delta_\pi-\tfrac{1}{4}\Delta_\pi(\cos\xi+\cos\eta)\,,\\
&(H^{\vec{k}}_{dd})_{22}=\tfrac{1}{2}\Delta_\pi-\tfrac{1}{4}\Delta_\pi(\cos\eta+\cos\zeta)\,,\\
&(H^{\vec{k}}_{dd})_{33}=\tfrac{1}{2}\Delta_\pi-\tfrac{1}{4}\Delta_\pi(\cos\zeta+\cos\xi)\,,
\end{aligned}
\tag{4.12}
$$

and

$$\Delta_\pi\equiv[-2\sqrt{2}\,(pd\pi)+2\sqrt{2}\,S_\pi E_{d\pi}]^2/(E_{d\pi}-E_{p\pi}). \tag{4.13}$$

The subscripts 1, 2, and 3 refer to the t_{2g} states xy, yz, and zx, respectively, according to the notation of Table III(I). Comparison with the results of this table suggest the introduction of an effective parameter D'_2 such that

$$D'_2=D_2-\tfrac{1}{8}\Delta_\pi\,. \tag{4.14}$$

Equations (4.11) and (4.14) illustrate a potential danger in attributing too much physical significance to the parameters which enter the LCAO or tight-binding interpolation scheme. Parameters which are intended to represent a d-d interaction can easily be dominated by p-d or s-d contributions. These contributions can determine both the sign and magnitude of the parameter. Evidence for such effects occurred in the determination of the parameter D_2 in the ReO_3 calculation, as described in I.

V. MO METHOD

The MO method has been applied by SS[6] and others[10,11] to calculate covalency effects and the crystal-field parameter Δ for the $(NiF_6)^{4-}$ molecular complex in the $KNiF_3$ crystal. The relationship between the ReO_3 and perovskite structures was described in I, where it was shown that the Ni and F atoms occupy the same positions as the Re and O atoms in ReO_3 while the K atoms are located at the corners of the cubic unit cell. Excellent reviews of MO theory, including its application to transition-metal compounds, are contained in the articles by Anderson[7] and Owen and Thornley.[12] These contain extensive references and trace the historical development of this field.

The MO approach differs from that of the LCAO (or more generally, the band) method in several important respects. First, the MO method neglects the lattice periodicity and considers only a

single molecular complex rather than the entire three-dimensional crystal. As a result, the MO method utilizes the point symmetry of this complex rather than the full space group of the crystal in order to factor the MO secular equation. In the case of an octahedral complex such as $(NiF_6)^{4-}$, the MO method includes only those bonding and antibonding orbitals which possess the octahedral point symmetry. For the ReO_3 and perovskite structures, these bonding and antibonding MO's correspond to LCAO Bloch states at Γ and R in the simple cubic Brillouin zone, respectively.

In order to clarify the relationship between the LCAO and MO methods, we summarize briefly the MO formalism of SS in terms of the LCAO parameters of Sec. III. In the band limit, this approach is equivalent to that of Sec. III. In the localized limit, this analysis reduces to the traditional MO formalism.

A. Band Limit

In their analysis, SS reduce the problem of calculating covalency effects and the crystal-field splitting Δ for the $(NiF_6)^{4-}$ complex to that of solving a pair of 2-by-2 secular equations involving nonorthogonal MO's, similar in form to those which result from the Hamiltonian and overlap matrices of Eq. (3.1). They apply a variational technique to solve these secular equations, introducing antibonding and bonding wave functions of the form

$$\Psi^a = N^{-1/2}(\varphi - \lambda\chi) , \tag{5.1a}$$

$$\Psi^b = N'^{-1/2}(\chi + \gamma\varphi) , \tag{5.1b}$$

which are exact eigenfunctions of the one-electron Hartree-Fock equation

$$H_{op}\Psi = E\Psi . \tag{5.2}$$

According to SS, φ is a normalized atomic d orbital localized at the metal ion, χ is the normalized MO wave function for the neighboring ligands, λ and γ are variational coefficients, and the N's are normalization constants. In the present treatment, the only new feature we introduce is that of replacing φ and χ by Bloch sums rather than using localized atomic and MO wave functions. When this is done, the ligand orbitals numbered 4–6 in Fig. 1 and Eq. (2.4) of Shulman and Sugano[13] are related to those numbered 1–3 by a lattice translation.

To determine the energies of the antibonding and bonding states, Ψ^a and Ψ^b are substituted into Eq. (5.2). Multiplying on the left-hand side by φ (and then χ) and integrating, we obtain

$$E^a_\alpha = [E_d - \lambda_\alpha\sqrt{6}\,(\alpha d\sigma)]/[1 - \lambda_\alpha\sqrt{6}\,S_\alpha] , \tag{5.3}$$

$$E^a_\alpha = [E_d - \lambda^2_\alpha E_\alpha]/(1 - \lambda^2_\alpha) , \tag{5.4}$$

and

$$E^b_\alpha = [E_\alpha + \gamma_\alpha\sqrt{6}\,(\alpha d\sigma)]/[1 + \gamma_\alpha\sqrt{6}\,S_\alpha] , \tag{5.5}$$

$$E^b_\alpha = [E_\alpha - \gamma^2_\alpha E_d]/(1 - \gamma^2_\alpha) , \tag{5.6}$$

which correspond to Eqs. (2.4)–(2.7) in SS. In Eqs. (5.3)–(5.6), we have used the Hamiltonian and overlap matrices of Eq. (3.1).

The variational parameters λ_α and γ_α are determined by equating the right-hand sides of Eqs. (5.3), (5.4) and (5.5), (5.6). By defining the dimensionless quantities

$$C_\alpha \equiv \tfrac{1}{2}\sqrt{6}\,S_\alpha , \tag{5.7}$$

$$D_\alpha \equiv -\sqrt{6}\,V_{\alpha d}/(E_d - E_\alpha), \tag{5.8}$$

and using Eq. (3.6), we find that

$$\lambda_\alpha = \tfrac{1}{2}(C_\alpha - D_\alpha)^{-1}\{1 - [1 - 4(C^2_\alpha - D^2_\alpha)]^{1/2}\} , \tag{5.9}$$

$$\gamma_\alpha = -\tfrac{1}{2}(C_\alpha + D_\alpha)^{-1}\{1 - [1 - 4(C^2_\alpha - D^2_\alpha)]^{1/2}\} . \tag{5.10}$$

By expanding the square root and rearranging terms, we obtain the equivalent expressions

$$\lambda_\alpha = (C_\alpha + D_\alpha)[1 + (C^2_\alpha - D^2_\alpha) + 2(C^2_\alpha - D^2_\alpha)^2 + \cdots] , \tag{5.11}$$

$$\gamma_\alpha = (-C_\alpha + D_\alpha)[1 + (C^2_\alpha - D^2_\alpha) + 2(C^2_\alpha - D^2_\alpha)^2 + \cdots] . \tag{5.12}$$

Keeping only the lowest-order terms and using Eqs. (5.7) and (5.8), we find the following approximate expressions for λ_α and γ_α:

$$\lambda_\alpha \approx \tfrac{1}{2}\sqrt{6}\,S_\alpha - \sqrt{6}\,V_{\alpha d}/(E_d - E_\alpha), \tag{5.13}$$

$$\gamma_\alpha \approx -\tfrac{1}{2}\sqrt{6}\,S_\alpha - \sqrt{6}\,V_{\alpha d}/(E_d - E_\alpha), \tag{5.14}$$

so that

$$\gamma_\alpha \approx \lambda_\alpha - \sqrt{6}\,S_\alpha , \tag{5.15}$$

which are equivalent to Eqs. (2.12)–(2.15) in SS. We point out that λ_α and $\gamma_\alpha (\alpha = s, p)$ correspond to $\sqrt{2}\lambda_\alpha$ and $\sqrt{2}\,\lambda_\alpha$ in SS. The factor $\sqrt{2}$ originates from the MO nature of their ligand wave function.

From Eqs. (5.13) and (5.14), we observe that the SS decomposition of the various contributions to the crystal-field parameter Δ [Eqs. (2.10) and (2.11) in SS] is ambiguous since the covalency parameter γ_α also has an overlap component $\frac{1}{2}\sqrt{6}\,S_\alpha$. The term $\sqrt{6}\,V_{\alpha d}/(E_d - E_\alpha)$ is more properly identified as the covalency contribution. Since $V_{\alpha d}$ is opposite in sign to S_α, we note that the overlap and covalency terms add in λ_α and cancel in γ_α.

In contrast to SS, we find that in the band approximation the overlap-covalency contributions to the crystal field from the $2s$ and $2p$ orbitals occur separately at different points in the Brillouin zone. Using Eqs. (3.14) and (5.4), we find that the shift in the e_g orbital energy due to s or p

overlap-covalency effects is given by

$$\Delta_\alpha = \lambda_\alpha^2 (E_d - E_\alpha)/(1-\lambda_\alpha^2) \ . \tag{5.16}$$

This result is exact if λ_α is evaluated using Eq. (5.9). It is similar in form to the expression for the crystal-field splitting which has been derived by Moriya, as described by Anderson [Eq. (6.15) of Ref. 7] in his review article on superexchange. This expression for Δ_α reduces to that given in Eq. (3.18) if λ_α^2 is neglected in the denominator of Eq. (5.16) and the approximate expression for λ_α in Eq. (5.13) is introduced in the numerator.

B. Localized Limit

The SS expressions for Δ contain $2s$, $2p\sigma$, and $2p\pi$ overlap and covalency contributions. In the band limit, we find that the $2s$ contribution Δ_s produces the crystal-field splitting of the t_{2g} and e_g bands while $\Delta_\sigma - \Delta_s$ is responsible for the e_g bandwidth. A corresponding contribution from the $2p\pi$ electrons causes the t_{2g} bandwidth. In Sec. VI, we shall find that the e_g and t_{2g} bandwidths are ~ 1 eV in $KNiF_3$. It is well known that in the limit where the bandwidth is small compared to the Coulomb energy U between two d electrons located on the same atom, the electrons will localize and form Wannier functions. In this way, the electrons sacrifice some kinetic energy that might be gained by delocalizing into Bloch states, but this kinetic-energy contribution to the total energy is small compared to the additional Coulomb terms U that would be introduced.

Anderson[7] has shown that the localized Wannier functions have the *average* energy of the band. From our perturbation treatment of the e_g and t_{2g} states in Sec. IV, we find from Eqs. (4.9) and (4.10) that the average energy for the e_g states $\langle E_e \rangle$ is given by

$$\langle E_e \rangle = E_{d\sigma} + \Delta_s + 3D_\Delta , \tag{5.17}$$

or using Eq. (4.8),

$$\langle E_e \rangle = E_{d\sigma} + \tfrac{1}{2}(\Delta_s + \Delta_\sigma) \ , \tag{5.18}$$

where we again introduce a second subscript σ on E_d and replace Δ_p by Δ_σ. According to Eq. (4.12), the average energy of the t_{2g}-band states $\langle E_t \rangle$ is given by

$$\langle E_t \rangle = E_{d\pi} + \tfrac{1}{2}\Delta_\pi \ , \tag{5.19}$$

where Δ_π is defined by Eq. (4.13).

In this localized limit, the crystal-field parameter $\Delta_{\rm loc}$ is defined as

$$\Delta_{\rm loc} \equiv \langle E_e \rangle - \langle E_t \rangle \ . \tag{5.20}$$

Introducing the results of Eqs. (5.18) and (5.19),

$$\Delta_{\rm loc} = E_{d\sigma} - E_{d\pi} + \tfrac{1}{2}(\Delta_s + \Delta_\sigma - \Delta_\pi). \tag{5.21}$$

Using the expressions for Δ_s, Δ_σ, and Δ_π given by Eqs. (3.19) and (4.13), it is straightforward to show that $\Delta_{\rm loc}$ of Eq. (5.21) is exactly equivalent to the expression for Δ that is given by SS in Eq. (2.10) or (2.11). Thus, we have shown that the MO method predicts the same crystal-field parameter as the LCAO method in the limit where U is large compared to the bandwidth.

VI. APPLICATION AND RESULTS

To simplify the discussion in this section and in Sec. VII, we introduce the following terminology. We refer to the Slater-Koster LCAO interpolation scheme involving orthogonalized orbitals as the linear-combination-of-"orthogonalized"-atomic-orbitals (LCOAO) method. The present method involving nonorthogonal orbitals is designated the LCAO method.

A. ReO_3

In principle, the application of the LCAO interpolation scheme to the ReO_3 band structure requires a reevaluation of the 19 LCOAO parameters introduced in I plus a determination of the four additional parameters that have been added in the present treatment. To simplify matters, we shall "freeze" 17 of the original 19 LCOAO parameters and modify only two of these. In particular, we modify $D_4 = E_{d\sigma}$ and $P_2 = (pd\sigma)$. The parameter D_4 is modified by assuming that $E_{d\sigma} = E_{d\pi} = D_1$, which removes all the crystal-field effects from the LCOAO treatment. The parameter E_s has been set equal to the energy of the top of the oxygen $2s$ band, as determined by the APW calculations described in I.

The four remaining parameters $(sd\sigma)$, S_s, $(pd\sigma)$, and S_σ have been determined by fitting the APW results for Γ_{12} and H_{12} exactly. In particular, $(sd\sigma)$ and S_s were determined by requiring that the eigenvalues of the secular equation that results from Eq. (3.3) with $\alpha = s$ reproduce the APW energies of the Γ_{12} states in the oxygen $2s$ and rhenium e_g bands. The parameters $(pd\sigma)$ and S_σ were determined in the same way by fitting the $2p\sigma$ and e_g states of H_{12} symmetry. In these calculations, the small d-d and p-p interaction terms that were omitted from the diagonal in Eq. (3.1a) were taken into account. The final values for all 23 LCAO parameters are listed in Table II.

In order to emphasize the difference between the LCOAO and LCAO schemes, we consider the results of Fig. 3. In Figs. 3(b) and 3(c), we compare the energy-band results along the [100] or Δ direction obtained by the LCOAO and LCAO methods, respectively. The corresponding APW results for ReO_3 are shown in Fig. 3(a). For orientation purposes, the bands that originate from the Γ_{12} and $\Gamma_{25'}$ states are the rhenium e_g and t_{2g} bands, respectively. The nine oxygen $2p$ bands are located about 0.2 Ry below the bottom of the t_{2g} band. The oxygen

TABLE II. Tight-binding parameters obtained by fitting the APW results for ReO_3 using the LCAO scheme with nonorthogonal orbitals.

Parameter	Value (Ry)	Parameter	Value (Ry)
A_1	−0.2761	$D_1 = D_4$	0.0592
A_2	0.0258	D_2	0.0000
A_3	−0.0034	D_3	−0.0001
B_1	−0.2294	D_5	−0.0241
B_2	−0.0191	D_6	0.0006
B_3	0.0049	$(pd\sigma)$	−0.2562
B_4	−0.0001	$(pd\pi)$	0.1324
C_1	0.0097	$(sd\sigma)$	−0.2849
C_2	0.0142	S_s	0.0988[a]
C_3	0.0034	S_σ	0.1105
C_4	−0.0037	E_s	−1.3400

[a] S_s and S_σ are dimensionless.

2s bands (which are not shown) extend from −1.34 to −1.43 Ry on this energy scale. The Γ_1-X_4, band near the top of Fig. 3(a) represents the lower portions of the rhenium 6s-6p conduction band. These states have been excluded from our tight-binding analysis and are therefore omitted from Figs. 3(b) and 3(c).

In Fig. 3(d), we show the results of an APW calculation in which the potential within the oxygen spheres has been set equal to zero. Roughly speaking, this is equivalent to a band calculation for simple cubic rhenium with an enormous lattice constant. Several differences are obvious between the results of Figs. 3(a) and 3(d). First, the crystal-field splitting between Γ_{12} and $\Gamma_{25'}$ has disappeared, and Γ_{12} actually lies lower than $\Gamma_{25'}$ in Fig. 3(d). Second, the 5d bands are quite flat, as one would expect from the large Re-Re separation.

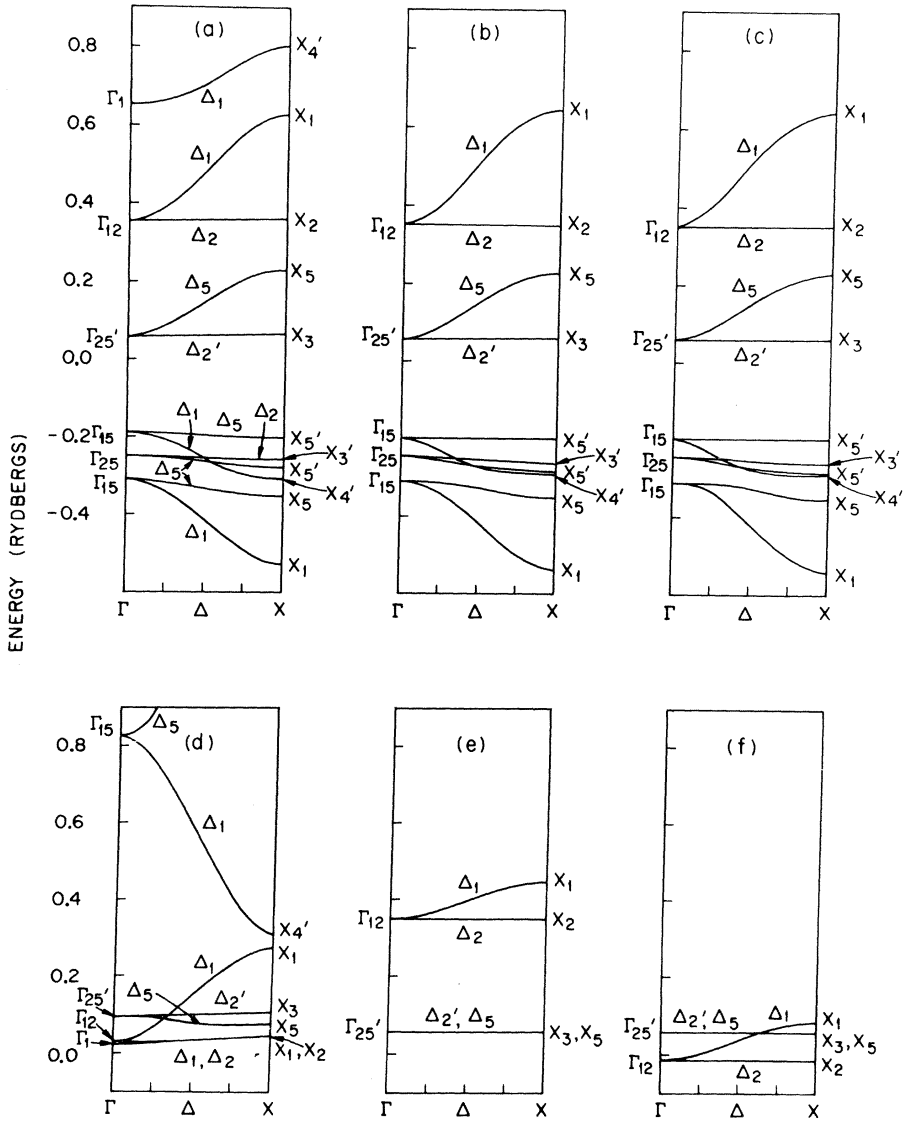

FIG. 3. (a) APW results for ReO_3 along the Δ line. (b) LCOAO results along Δ. (c) LCAO results. (d) APW results with zero potential within oxygen spheres. (e) LCOAO results with zero covalency. (f) LCAO results with zero overlap and covalency.

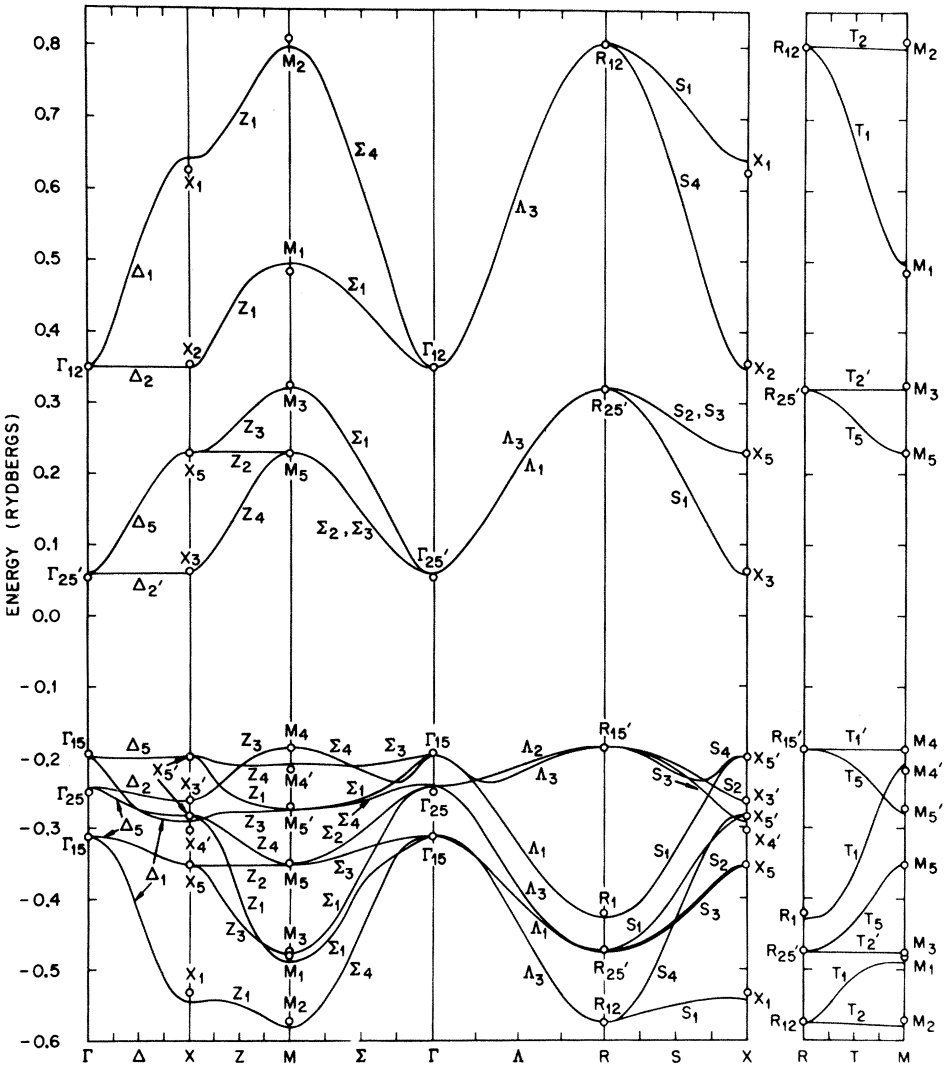

FIG. 4. LCAO energy bands for ReO_3.

Finally, the rhenium $6s$-$6p$ bands have dropped down in energy until Γ_1 is slightly below the $5d$ bands at the zone center Γ. This is a familiar feature of transition-metal band structures.

The results shown in Figs. 3(e) and 3(f) represent an attempt to simulate the APW results of Fig. 3(d) in the LCOAO and LCAO approximations. In obtaining the results shown in Fig. 3(e), the $2p$-$5d$ interaction parameters $(pd\sigma)$ and $(pd\pi)$ in the LCOAO calculation have been set equal to zero. The corresponding results shown in Fig. 3(f) were obtained by setting S_s, S_σ, $(sd\sigma)$, $(pd\sigma)$, and $(pd\pi)$ equal to zero in the LCAO calculation. Unlike the LCOAO results of Fig. 3(e), the crystal-field splittings disappear in the LCAO results of Fig. 3(f) and the resulting $5d$ bands resemble rather closely the APW results in Fig. 3(d). The small differences between the Δ_1 and Δ_5 bands are easily attributed to $6s$-$6p$ hybridization, which is automatically included in the APW calculation but not in our LCAO scheme.

Although the rhenium $6s$-$6p$ bands have not been treated explicitly in the present LCAO analysis, it is clear from the results of Fig. 3 that these states are shifted to higher energies in Fig. 3(a) by the same overlap-covalency effects which are responsible for the crystal-field splittings in the rhenium $5d$ bands.

The over-all features of the LCAO fit to the APW results for ReO_3 are shown in Fig. 4. Here, $E(\vec{k})$ curves along symmetry lines of the simple cubic Brillouin zone represent the LCAO bands. The APW results at symmetry points which have been used to determine the LCAO parameters are indicated by the open circles. This LCAO method has reduced the maximum deviation between the APW and the previous LCOAO results from about 0.04 Ry to less than 0.02 Ry. This modest improvement

TABLE III. Comparison between the APW results for ReO_3 and those obtained via the LCAO interpolation scheme using orthogonal (LCOAO) and nonorthogonal (LCAO) orbitals.

State	APW	LCOAO	LCAO	State	APW	LCOAO	LCAO
Γ_{12}	0.351	0.351	0.351	R_{12}	0.803	0.776	0.803
$\Gamma_{25'}$	0.055	0.059	0.059	$R_{25'}$	0.322	0.321	0.321
Γ_{15}	−0.193	−0.198	−0.198	$R_{15'}$	−0.189	−0.187	−0.187
Γ_{25}	−0.250	−0.243	−0.243	R_1	−0.421	−0.428	−0.428
Γ_{15}	−0.311	−0.313	−0.313	$R_{25'}$	−0.473	−0.476	−0.476
Γ_{12}	−1.428	...	−1.428	R_{12}	−0.574	−0.541	−0.574
X_1	0.626	0.646	0.643	M_2	0.811	0.775	0.798
X_2	0.356	0.349	0.349	M_1	0.487	0.506	0.496
X_5	0.230	0.230	0.230	M_3	0.328	0.321	0.321
X_3	0.064	0.059	0.059	M_5	0.229	0.230	0.230
$X_{5'}$	−0.20	−0.199	−0.199	M_4	−0.186	−0.188	−0.188
$X_{3'}$	−0.260	−0.263	−0.263	$M_{4'}$	−0.218	−0.211	−0.211
$X_{5'}$	−0.282	−0.283	−0.283	$M_{5'}$	−0.270	−0.277	−0.277
$X_{4'}$	−0.303	−0.292	−0.292	M_5	−0.350	−0.352	−0.352
X_5	−0.353	−0.352	−0.352	M_3	−0.474	−0.477	−0.477
X_1	−0.532	−0.539	−0.543	M_1	−0.480	−0.494	−0.489
X_2	−1.432	...	−1.428	M_2	−0.571	−0.551	−0.581
X_1	−1.444	...	−1.372	M_1	−1.437	...	−1.401

in accuracy is expected since the present LCAO method includes four additional fitting parameters.

A detailed comparison between the APW results for ReO_3 and those obtained by the LCOAO and LCAO fitting procedures is contained in Table III. Since we have frozen most of the LCOAO parameters, only those states which interact with or form the rhenium e_g bands have been modified in the LCAO calculation.

It is instructive to examine the relative magnitudes of some of the parameters listed in Table II. For example, we note that the $2p\sigma$-$5d$ overlap integral S_σ is slightly larger than the $2s$-$5d$ overlap integral S_s. This difference is consistent with the radial charge distribution of the Herman-Skillman[14] atomic wave functions for the oxygen $2s$ and $2p$ states. If one plots the radial portion of these functions for neutral oxygen, it is found that the amplitudes of the $2s$ and $2p$ orbitals are nearly equal at the oxygen sphere radius. However, the lower energy of the $2s$ orbital causes it to decrease more rapidly than the $2p$ function at larger distances.

We can also understand the relative magnitudes of $(sd\sigma)$ and $(pd\sigma)$ in terms of Eq. (3.6). In the case of $(sd\sigma)$, the results of Table II and Eq. (3.6) yield the result that

$$(sd\sigma) = \tfrac{1}{2} S_s(E_s + E_d) + V_{sd} = -(0.0667 + 0.2182)\ \text{Ry}. \quad (6.1)$$

Similarly, for $(pd\sigma)$ we find

$$(pd\sigma) = \tfrac{1}{2} S_\sigma(E_p + E_d) + V_{pd} = -(0.0071 + 0.2491)\ \text{Ry}. \quad (6.2)$$

Thus, the parameters V_{sd} and V_{pd} scale accurately with the overlap integrals S_s and S_σ. The ratios V_{sd}/S_s and V_{pd}/S_σ are -2.21 and -2.25 Ry, respectively. The large negative value for E_s in Eq. (6.1) is responsible for the fact that $|(sd\sigma)| > |(pd\sigma)|$.

Using the results of Table II, we can now determine the magnitudes of the various terms in Eq. (3.11) when it is applied to the Γ_{12} and R_{12} states. The results are summarized in Table IV. For purposes of comparison, we have also included in this table the analogous results for the Γ_1 states in the oxygen $2s$ and rhenium $6s$ bands. For this case, the parameters are given without subscripts. [These states lead to a Hamiltonian matrix with the same form as $\underline{H'}$ in Eq. (3.11), except that $\sqrt{6}\,S_\alpha$ and $\sqrt{6}\,V_{\alpha d}$ are replaced by $2\sqrt{3}\,S$ and $2\sqrt{3}\,V$, respectively]. From the results of Table IV, A_s and A_p are found to be much smaller than the terms $\frac{1}{2} B_s$ and $\frac{1}{2} B_p$. The same is true for the relative magnitudes of A and $\frac{1}{2} B$. Furthermore, we note that the magnitude of the off-diagonal matrix element $\frac{1}{2} B_p/\sqrt{6}\,S_p$ relative to the energy denominator $(E_d - E_p)$ precludes the possibility of treating the $2p$-$5d$ interaction in ReO_3 by second-order perturbation theory. The situation is only slightly more favorable for the $2s$-$5d$ and $2s$-$6s$ interactions because of the larger energy denominators.

From an analysis of the Γ_1 states, we find that $(ss\sigma) = -0.2590$ Ry, $S = 0.0980$, and $V = -0.1946$ Ry. The ratio $V/S = -1.99$ Ry is within 10% of the previously quoted values for V_{sd}/S_s and V_{pd}/S_σ.

B. $KNiF_3$

To apply the LCAO method to $KNiF_3$, we deter-

TABLE IV. Values for the various terms (in rydbergs) of Eq. (3.11) when applied to Γ_{12} and R_{12}, using the parameters of Table II. The analogous results for Γ_1 are also included.

$E_d(\Gamma_{12})$ [a]	−0.0113	$E_d(R_{12})$ [b]	0.1297
E_s	−1.3400	$E_p(R_{12})$ [c]	−0.2573
A_s	0.0203	A_p	0.0075
$\frac{1}{2}B_s$	0.1374	$\frac{1}{2}B_p$	0.1783
$\frac{1}{2}B_s/\sqrt{6}\,S_s$	0.5678	$\frac{1}{2}B_p/\sqrt{6}\,S_p$	0.6584
$E_{6s}(\Gamma_1)$	0.0249		
E_s	−1.3400		
A	0.0431		
$\frac{1}{2}B$	0.2587		
$\frac{1}{2}B/2\sqrt{3}\,S$	0.7619		

[a] $E_d(\Gamma_{12}) = D_1 + 3(D_5 + D_6)$.
[b] $E_d(R_{12}) = D_1 - 3(D_5 + D_6)$.
[c] $E_p(R_{12}) = A_1 - 2A_2 - 4A_3 + 4C_2$.

TABLE V. LCAO parameters for $KNiF_3$ and their relation to the MO integrals of SS.

SS	Value[a]	LCAO
$(\varphi_{t_{2g}} \mid h_0 \mid \varphi_{t_{2g}})$	0.273 0	D_1
$(\varphi_{e_g} \mid h_0 \mid \varphi_{e_g})$	0.240 4	D_4
$(\chi_s \mid h_0 \mid \chi_s)$	−1.991 8	E_s
$(\chi_{p\sigma} \mid h_0 \mid \chi_{p\sigma})$	−0.325 6	A_1
$(\chi_{p\pi} \mid h_0 \mid \chi_{p\pi})$	−0.167 0	B_1
$(\varphi_{e_g} \mid h_0 \mid \chi_s)$	−0.232 0	$\sqrt{3}\,(sd\sigma)$
$(\varphi_{e_g} \mid h_0 \mid \chi_{p\sigma})$	−0.197 2	$\sqrt{3}\,(pd\sigma)$
$(\varphi_{t_{2g}} \mid h_0 \mid \chi_{p\pi})$	−0.088 6	$-2(pd\pi)$
$(\varphi_{e_g} \mid \chi_s)$	0.081 43	$\sqrt{3}\,S_s$
$(\varphi_{e_g} \mid \chi_{p\sigma})$	0.110 71	$\sqrt{3}\,S_\sigma$
$(\varphi_{t_{2g}} \mid \chi_{p\pi})$	0.075 57	$-2S_\pi$

[a] Integrals containing the Hamiltonian h_0 are in Ry, the overlap integrals are dimensionless.

mine the various LCAO parameters from the MO integrals tabulated in Table VI of SS.[6] The eleven LCAO parameters that are used in this calculation for $KNiF_3$ are listed in Table V. To maintain a consistent set of units in the present paper, we have converted the SS values from a.u. to Ry. The relationship between the SS integrals and the LCAO parameters is given explicitly. The factors $\sqrt{3}$ and 2 arise from the MO nature of the χ orbitals. The change in sign for $(pd\pi)$ and the corresponding overlap integral S_π is introduced in order to maintain our choice of phase, as illustrated in Fig. 1(c). The form of the π overlap matrix is readily obtained from the results of Table III (I) by replacing $H_{i,j}$ and P_1 by $S_{i,j}$ and S_π, respectively.

Using these parameters, we obtain the LCAO band structure for $KNiF_3$ that is shown in Fig. 5. A comparison with the previous results for ReO_3 in Fig. 4 suggests many similarities. As far as the Ni $3d$ bands are concerned, the crystal-field splitting $E(\Gamma_{12}) - E(\Gamma_{25'})$ is smaller than the t_{2g} bandwidth $E(X_5) - E(X_3)$, and this produces overlap of the t_{2g} and e_g bands. In this respect, the $KNiF_3$ $3d$ bands are similar to those obtained by Kahn and Leyendecker for the conduction bands in

TABLE VI. LCAO wave functions for the bonding and antibonding states that form and interact with the e_g bands in ReO_3 and $KNiF_3$.

					ReO_3					$KNiF_3$
k	State	s	p	d	C_s	C_p	C_d	C_s	C_p	C_p
(0, 0, 0)	Γ_{12}^s	Φ_{s1} [a]	···	$3z^2-r^2$	0.9197	···	0.2288	0.9940	···	0.0436
	Γ_{12}^s	Φ_{s2} [b]	···	x^2-y^2	0.9197	···	0.2288	0.9940	···	0.0436
	Γ_{12}^d	Φ_{s1}	···	$3z^2-r^2$	−0.4652	···	1.0049	−0.1591	···	1.0058
	Γ_{12}^d	Φ_{s2}	···	x^2-r^2	−0.4652	···	1.0049	−0.1591	···	1.0058
(0, 0, π/a)	X_1^s	$-\Phi_{s3}$ [c]	$-iz_3$	$3z^2-r^2$	0.9681	0.0294	0.1446	0.9980	−0.0004	0.0254
	X_1^p	$-\Phi_{s3}$	$-iz_3$	$3z^2-r^2$	−0.1721	0.8147	0.4192	−0.0269	0.9314	0.2641
	X_1^d	$-\Phi_{s3}$	$-iz_3$	$3z^2-r^2$	−0.2327	−0.6227	0.9363	−0.0884	−0.3861	0.9751
	X_2^s	Φ_{s2}	···	x^2-y^2	0.9195	···	0.2291	0.9940	···	0.0436
	X_2^d	Φ_{s2}	···	x^2-y^2	−0.4655	···	1.0049	−0.1591	···	1.0058
(π/a, π/a, 0)	M_1^s	s_3	Φ_{p3} [d]	$3z^2-r^2$	0.9417	0.0275	0.1952	0.9960	−0.0004	0.0358
	M_1^p	s_3	Φ_{p3}	$3z^2-r^2$	−0.1805	0.8914	0.3247	−0.0284	0.9624	0.1986
	M_1^d	s_3	Φ_{p3}	$3z^2-r^2$	−0.3497	−0.4803	0.9614	−0.1271	−0.2865	0.9882
	M_2^p	···	$-\Phi_{p2}$ [e]	x^2-y^2	···	0.7470	0.4926	···	0.9051	0.3065
	M_2^d	···	$-\Phi_{p2}$	x^2-y^2	···	−0.7218	0.9145	···	−0.4538	0.9650
(π/a, π/a, π/a)	R_{12}^p	···	$-\Phi_{p1}$ [f]	$3z^2-r^2$	···	0.7426	0.4982	···	0.9051	0.3065
	R_{12}^p	···	$-\Phi_{p2}$	x^2-y^2	···	0.7426	0.4982	···	0.9051	0.3065
	R_{12}^d	···	$-\Phi_{p1}$	$3z^2-r^2$	···	−0.7263	0.9115	···	−0.4538	0.9650
	R_{12}^d	···	$-\Phi_{p2}$	x^2-y^2	···	−0.7263	0.9115	···	−0.4538	0.9650

[a] $\Phi_{s1} = (6)^{-1/2}(2s_3 - s_1 - s_2)$.
[b] $\Phi_{s2} = (2)^{-1/2}(s_1 - s_2)$.
[c] $\Phi_{s3} = (2)^{-1/2}(s_1 + s_2)$.
[d] $\Phi_{p3} = i(2)^{-1/2}(x_1 + y_2)$.
[e] $\Phi_{p2} = i(2)^{-1/2}(x_1 - y_2)$.
[f] $\Phi_{p1} = i(6)^{-1/2}(2z_3 - x_1 - y_2)$.

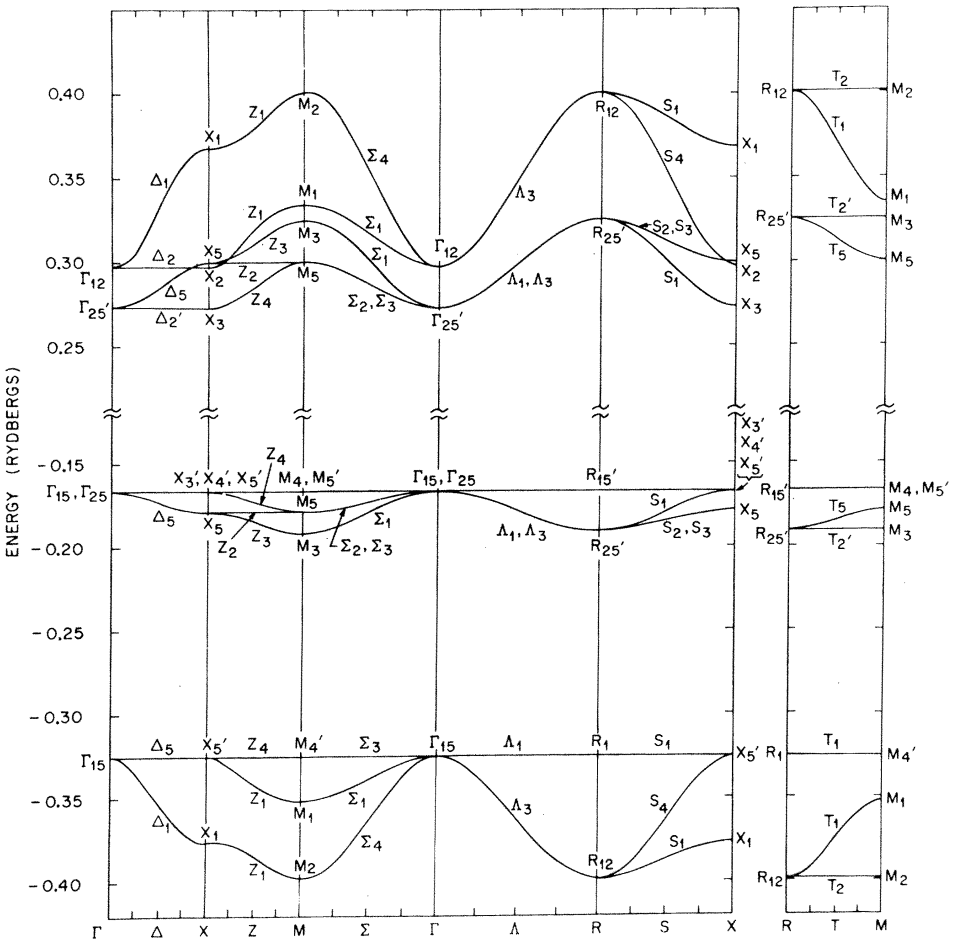

FIG. 5. LCAO energy bands for $KNiF_3$.

$SrTiO_3$.[15]

The fluorine $2p$ valence bands exhibit several features which are quite different from those of the oxygen $2p$ bands in ReO_3. The most obvious of these is the fact that the three $2p\sigma$ bands are split off from the six $2p\pi$ bands by about 0.16 Ry. Covalency effects in the $2p\pi$ bands reduce the actual gap to about 0.13 Ry. The corresponding bandwidth induced in the $2p\sigma$ bands by the stronger $(pd\sigma)$ interaction is about 0.07 Ry. Since neither the present APW results for ReO_3 nor preliminary APW results for $SrTiO_3$ exhibit this degree of splitting between the $2p\sigma$ and $2p\pi$ valence bands, we view this feature of the $KNiF_3$ band structure with suspicion.

If the LCAO parameters $(sd\sigma)$ and $(pd\sigma)$ for $KNiF_3$ are decomposed according to Eq. (3.6), the resulting values for V_{sd} and V_{pd} again scale with the overlap integrals S_s and S_σ. In this case, the ratios V_{sd}/S_s and V_{pd}/S_σ are -1.97 and -1.74 Ry, respectively. If Eq. (3.6) is generalized to represent the $(pd\pi)$ integral, the corresponding ratio $V_{pd\pi}/S_\pi = -1.22$ Ry. Furthermore, we find for $KNiF_3$ that the relative magnitudes of the various overlap-covalency terms that are shown schematically in Fig. 2 compare favorably with the ReO_3 results that are listed in Table IV. However, the magnitude of the parameters Δ_α is reduced because of the smaller degree of covalency and overlap in $KNiF_3$.

C. Wave Functions

We examine the detailed nature of the LCAO wave functions for ReO_3 and $KNiF_3$ to determine the extent of covalency in the bonding orbitals and its consequences on their antibonding partners. These results allow us to examine critically the accuracy of second-order perturbation theory in the calculation of covalency and crystal-field effects in these materials.

The LCAO wave functions for the $2s$, $2p\sigma$, and e_g states of ReO_3 and $KNiF_3$ at symmetry points in the Brillouin zone are tabulated in Table VI. The eigenvectors C_s, C_p, and C_d are equivalent to those obtained by solving Eq. (4.1) exactly. In terms of Eq. (5.1a), the antibonding wave function for $\Gamma_{12}(\Gamma_{12}^d)$ indicates that $N^{-1/2} = C_d$ and $N^{-1/2}\lambda = -C_s$. For the bonding state Γ_{12}^s, Eq. (5.1b) suggests that

TABLE VII. Comparison between the exact and second-order perturbation theory (PT) results for λ_α, γ_α, and Δ_α for ReO_3 and $KNiF_3$.

	ReO_3		$KNiF_3$	
	Exact	PT	Exact	PT
$\gamma_s(\Gamma_{12}^s)$	0.249	0.281	0.044	0.044
$\lambda_s(\Gamma_{12}^d)$	0.463	0.523	0.158	0.159
$\gamma_\sigma(R_{12}^p)$	0.671	1.441	0.339	0.403
$\lambda_\sigma(R_{12}^d)$	0.797	1.712	0.470	0.560
$\gamma_\pi(R_{25'}^p)$	···	···	−0.226	−0.244
$\lambda_\pi(R_{25'}^d)$	···	···	−0.325	−0.351
$\Delta_s(\Gamma_{12})$ [a]	0.363	0.364	0.057	0.057
$\Delta_\sigma(R_{12})$	0.673	1.134	0.161	0.177
$\Delta_\pi(R_{25'})$	···	···	0.052	0.054
$\Delta_{\rm loc}(\rm cm^{-1})$	···	···	5530	6340

[a] Δ_s, Δ_σ, and Δ_π are in Ry.

$N'^{-1/2}=C_s$ and $N'^{-1/2}\gamma=C_d$. The normalization for these wave functions is such that $C_s^2+2\sqrt{6}S_\alpha C_s C_d + C_d^2=1$.

A superficial comparison between the results for ReO_3 and $KNiF_3$ demonstrates that the covalency is much stronger in the former compound. It is also clear that the degree of covalency varies throughout the Brillouin zone and depends critically on the symmetry of the states involved. These results also exhibit the approximate relationship between the covalency γ_α, the overlap $\sqrt{6}S_\alpha$, and the variational parameter λ_α that is given by Eq. (5.15) for the states at Γ and R, namely, $\lambda_\alpha \approx \gamma_\alpha + \sqrt{6}S_\alpha$.

A comparison is made in Table VII between the exact and perturbation-theory values of γ, λ, and Δ for ReO_3 and $KNiF_3$. The exact values are obtained from Eqs. (5.9), (5.10), and (5.16) while the approximate values result from Eqs. (5.13), (5.14), and (5.16) if λ_α^2 is neglected in the denominator of the last equation. These equations also are valid for the π interactions if $\sqrt{6}S_\alpha$ and $\sqrt{6}V_{\alpha d}$ are replaced by $2\sqrt{2}S_\pi$ and $2\sqrt{2}V_{pd\pi}$, respectively.

Second-order perturbation theory is reasonably accurate in $KNiF_3$, but breaks down when applied to the p-d interactions in ReO_3. Even in $KNiF_3$, the use of perturbation theory introduces a 10% error in Δ_σ. According to Eq. (5.21), Δ_σ represents the principal positive contribution to $\Delta_{\rm loc}$ since Δ_s and Δ_π nearly cancel and $E_{d\sigma}$-$E_{d\pi}$ is negative in the SS calculation. Thus, the exact values for λ yield a value for $\Delta_{\rm loc}$ which is about 15% smaller than the SS value of 6340 $\rm cm^{-1}$.

VII. SUMMARY AND DISCUSSION

We shall not attempt to review the various theories on the origin of crystal-field splittings in transition-metal complexes and compounds since comprehensive review articles already exist in the literature.[7,12] Generally speaking, we can use Anderson's classification and characterize these theories as the ionic and partially covalent theories.[7] According to the ionic theory, the crystal-field splitting is due to the electrostatic field of negatively charged ligands which surround the transition-metal ion. The covalent theories attribute these crystal-field effects to wave-function overlap and the formation of partially covalent bonds between the transition-metal d and the ligand s and p orbitals. It should be clear from the results of the previous sections that the present LCAO approach represents an extension and generalization of the MO method for calculating the overlap-covalency contributions to the crystal-field parameters.

We have shown that the LCAO and MO methods yield quite different results in the limit where the one-electron band theory provides a valid description of the d states. In this limit, the selection rules that are imposed by the additional quantum number $\vec{k}$ decompose the MO crystal-field parameter $\Delta_{\rm loc}$ into three distinct parameters Δ_s, Δ_σ, and Δ_π. The influence of these parameters on the d bands is both wave-vector and crystal-structure dependent. In the case of the ReO_3 and perovskite structures, these parameters not only are responsible for the crystal-field-type splittings that tend to separate the e_g and t_{2g} bands, but they also determine the e_g and t_{2g} bandwidths as well. In a sense, the LCOAO method attempts to introduce this crystal-field splitting in a way that is analogous to that of the MO method. Namely, the crystal-field effects are included as a rigid shift of the e_g band relative to the t_{2g} states that is independent of the wave vector $\vec{k}$. The covalency effects which are due to the $(pd\sigma)$ and $(pd\pi)$ interactions are treated separately. The LCAO method treats these effects in a more uniform manner and determines the detailed relationship that exists between crystal-field effects, covalency, and overlap.

It is important to emphasize that the addition of oxygen 2s orbitals to the LCOAO treatment of ReO_3 in I will not provide a more satisfactory representation of the crystal-field effects in this compound. These effects require the asymmetrical splitting that results from orthogonalization in the LCAO method. This is clear from the combined results of Figs. 2–4. According to Figs. 3(d) and 4, the rhenium 5d and oxygen 2p bands each have a natural width of about 0.1 Ry that is due to d-d and p-p interactions, respectively. Yet overlap and covalency effects increase the 5d bandwidth until it is about twice that of the oxygen 2p band. The origin of this asymmetry is illustrated schematically in Fig. 2. There, it is shown that the total shift of the d-state energy is greater than that of the valence-band state because the latter shift is reduced by cancellation effects among the various overlap-covalency terms. The final valence and

d-band energies shown to the right are displaced symmetrically with respect to the diagonal energies of the orthogonal orbitals E'_α and E'_d but not with respect to E_α and E_d. This asymmetry can only be introduced into the LCOAO method by shifting the center of gravity of the e_g bands relative to that of the t_{2g} bands.

We have noted that it is only in the limit where the Coulomb interaction energy U is comparable with the e_g and t_{2g} bandwidths that the MO and LCAO methods yield identical results for the crystal-field parameter Δ. In this limit, it is energetically favorable for Bloch waves to localize into Wannier functions in order to minimize the Coulomb interactions. It is important to emphasize that these localized Wannier functions are associated with a finite virtual bandwidth. This virtual bandwidth is related directly to the effective transfer integral b which enters Anderson's theory of superexchange.[7] If the energy bands were perfectly flat, then b would be zero and there would be no antiferromagnetic exchange coupling between the localized spins on neighboring transition-metal ions.

According to Anderson's theory, this antiferromagnetic coupling between neighboring transition-metal ions can be represented in terms of a Heisenberg interaction

$$-J_{\text{eff}}\vec{S}_1\cdot\vec{S}_2 \ , \tag{7.1}$$

where J_{eff} is an effective exchange integral,[12]

$$J_{\text{eff}} = (s^2/S^2)(4b^2/U) \ . \tag{7.2}$$

In Eq. (7.2), $s=\frac{1}{2}$ and S corresponds to the total spin of the ion. For the e_g states, b is readily shown to be equal to $\frac{1}{6}(\Delta_\sigma - \Delta_s)$, where Δ_α is given by Eq. (5.16). According to Eq. (4.8), b is also equal to D_Δ. To second order in λ_α,

$$b = \tfrac{1}{6}[\lambda_\sigma^2(E_d - E_p) - \lambda_s^2(E_d - E_s)] \ , \tag{7.3}$$

which is similar to Anderson's Eq. (7.10) except that he has the quantities $(\lambda_\sigma^2 - S_\sigma^2)$ and $(\lambda_s^2 - S_s^2)$ multiplying the energy differences $(E_d - E_p)$ and $(E_d - E_s)$, respectively.

Using the exact values of Δ_s and Δ_σ for $KNiF_3$ from Table VII, setting $U=8$ eV and $S=1$, we find that $J_{\text{eff}} = 80\ ^\circ\text{K}$. This is close to the value of $76\ ^\circ\text{K}$ that is quoted by Anderson, the result of an unpublished calculation by Moriya, Shulman, Sugano, and Anderson. Owen and Thornley[12] point out that Anderson's expression for J_{eff} contains an additional factor of $\frac{1}{2}$ which they do not understand. Thus, these two results actually differ by nearly a factor of 2. This difference is due to the fact that the perturbation-theory value for λ_σ used by Moriya *et al.* is 20% larger than the exact value, according to the results of Table VII. This is compensated, to some extent, by the fact that Moriya *et al.* use $N^{-1/2}\lambda_\sigma$ and $N^{-1/2}\lambda_s$ rather than λ_σ and λ_s in their calculation of b. From the experimental values for the Néel point T_N and the susceptibility at the Néel point $\chi(T_N)$, Smart finds an empirical value of $45\ ^\circ\text{K}$ for $KNiF_3$.[16]

We comment briefly on the origin of the extra factors S_σ^2 and S_s^2 that occur in Anderson's expression for b. These additional terms arise from the application of Phillips's cancellation theorem[17] to the energy difference between the symmetric and antisymmetric d-orbital combinations. We find that this difference is zero in the localized Wannier function limit since both combinations have the same average band energy. According to Phillips's theorem, metal-ligand overlap effects accurately cancel the excess attractive potential that results when point-ion ligands are replaced by distributed-charge ligands, thereby justifying the use of the point-ion approximation in crystal-field calculations.

It is important to note that the same overlap-covalency mechanism is capable of explaining the crystal-field effects in a metallic nonmagnetic system such as ReO_3 as well as a semiconducting antiferromagnetic material such as $KNiF_3$. We conclude that the methods of the covalency approach can be applied to a wide variety of compounds. Although the point-ion model often yields results which are in fair agreement with experiment, we tend to regard this success as accidental rather than fundamental.

The results of this LCAO approach suggest that APW band calculations could represent a valuable tool for providing theoretical estimates of Δ for a variety of compounds. In general, the APW method is easier to apply than MO theory since it eliminates the evaluation of complicated two- and three-center integrals which occur in the MO method. Furthermore, these band calculations can also provide fairly accurate estimates of the bandwidth. A systematic band-structure study of the various fluoride and oxide systems could indicate the variation of U in the $3d$, $4d$, and $5d$ transition series. For example, the optical studies by Knox, Shulman, and Sugano[18] on $KNiF_3$ and $KMgF_3$: 0.10Ni^{2+} clearly imply a localized model in which $b/U<1$. On the other hand, the Fermi surface data for ReO_3 imply[3,4] that $b/U>1$ in this compound. In this way, calculated values for b can be used to set upper and lower limits on U.

Anderson[7] estimates that $U=9\pm2$ eV for the latter members of the $3d$ transition series. It is interesting to consider the question of why U should be so much larger in the transition-metal oxides and fluorides than it is in the transition metals. The $3d$ bandwidth in $KNiF_3$ is certainly comparable with that of fcc nickel, for example. I suggest two possible explanations. The first involves the fact that the same overlap-covalency mechanism that is re-

sponsible for crystal-field effects in the transition-metal compounds also raises the low-mass s-p conduction bands to higher energies. Whereas the lower portions of these bands are filled in the transition metals, they remain unoccupied in these compounds. As a result, the d-d Coulomb interaction in the compound cannot be screened by the relatively mobile s-p electrons that are available in the metal.

A second explanation involves the energy dependence of the d radial functions. Wood[19] has shown that in the solid, the d radial functions near the bottom of the d bands are relatively diffuse compared to atomic d orbitals. However, those near the top of the d band are slightly more compact than the atomic functions. In the transition-metal compounds, the crystal-field effects which raise the e_g orbital energy tend to compress their d radial charge distribution even further; this effect would certainly tend to increase the magnitude of U.

In I, the LCOAO wave functions were used to estimate the charge distribution in ReO_3. Assuming that the orthogonalized oxygen $2p$ and rhenium $5d$ orbitals were completely localized about their respective sites, this LCOAO calculation implied a charge distribution of $(Re^{+4})\,(O^{-4/3})_3$. Since the orthonormal functions $\psi_n(\vec{r})$ that are included in this LCOAO calculation actually represent linear combinations of the nonorthogonal orbitals $\varphi_n(\vec{r})$, this result represents an upper limit to the true ionicity. The results of the present LCAO analysis demonstrate that appreciable covalency and overlap occur between the rhenium and oxygen atoms in ReO_3, even in the tightly bound oxygen $2s$ band. The APW results of Fig. 3 and their interpretation in Sec. VI A indicate that the effects of the rhenium $6s$ and $6p$ states on the oxygen $2s$ and $2p$ bands cannot be entirely neglected. In view of this situation, one wonders if these materials are ionic at all. Perhaps these compounds obey the charge-neutrality principle of Pauling[20,21]: "The electronic structure of stable molecules and crystals is such that the electronic charge of each atom is close to zero."

Next we consider the decomposition of the metal-ligand interaction $(\alpha d\sigma)$ that is represented by Eq. (3.6) Originally, this relation was introduced for the primary purpose of simplifying the matrix elements of $\underline{H}'$ that are given by Eq. (3.3). According to results of Eq. (3.7), this decomposition possesses additional merit. Namely, it yields expressions for the matrix elements of $\underline{H}'$ which are independent of the zero of energy. This feature extends to other expressions involving $(\alpha d\sigma)$ or $V_{\alpha d}$, including Eqs. (3.18) and (3.19) for Δ_α. As a result, we consider $V_{\alpha d}$ to be the more fundamental of the two parameters since the sign and magnitude of $(\alpha d\sigma)$ depend on the choice of a zero of energy while $V_{\alpha d}$ is independent of this choice. In Sec. VI A, it is more precise to state that V_{sd} and S_s (V_{pd} and S_σ) for ReO_3 were determined by fitting the APW results for Γ_{12} (R_{12}) with the eigenvalues of Eq. (3.7) with $\alpha = s(p)$ and then $(sd\sigma)$ $[(pd\sigma)]$ was determined using Eq. (3.6). The accuracy with which V_{sd} and V_{pd} scale with the overlap integrals S_s and S_σ supports this point of view.

According to the results of Eqs. (6.1) and (6.2), $V_{\alpha d}$ completely dominates the $\frac{1}{2}S_\alpha(E_\alpha + E_d)$ contribution to $(\alpha d\sigma)$. Therefore, we consider Eq. (3.6) to be a more accurate representation of this metal-ligand interaction than the Wolfsberg-Helmholz formula[22]

$$H_{ij} = \tfrac{1}{2}FS(H_{ii} + H_{jj}) \ . \tag{7.4}$$

Here, F is a constant that is usually equal to about 2; H_{ii} and H_{jj} are equivalent to E_α and E_d in the present notation. With $F = 2$, the Wolfsberg-Helmholz formula requires that

$$V_{\alpha d} = \tfrac{1}{2}S_\alpha(E_\alpha + E_d) \ ,$$

which is in disagreement with our findings.

It should be pointed out that the present LCAO method can be formulated in terms of pseudopotentials. In such an approach, the d orbitals $\varphi_n(\vec{r})$ are orthogonalized explicitly to the neighboring s and p ligand orbitals $\varphi_t(\vec{r})$:

$$\psi_n(\vec{r}) = \varphi_n(\vec{r}) - \textstyle\sum_t (\varphi_t \mid \varphi_n)\,\varphi_t(\vec{r}) \ , \tag{7.5}$$

where $(\varphi_t \mid \varphi_n)$ is the metal-ligand overlap integral. Herring[23] has pointed out that a fictitious repulsive potential around each neighboring ligand atom could be introduced to represent the energetic effect of the "nodes and loops" required by orthogonalization and contribute to the crystal-field splitting. However, I believe that the present LCAO method is more direct and convenient since it preserves the simple form of the LCOAO Hamiltonian matrix in I by introducing the minor inconvenience of a non-diagonal overlap matrix.

It is difficult to estimate the accuracy of the LCAO parameters for ReO_3 that are listed in Table II. Some errors could easily be introduced by the approximation of "freezing" 17 of the original 19 LCOAO parameters. The results of Fig. 3 suggest that these errors are not serious. Our analysis indicates that the π overlap integral is not entirely negligible in ReO_3. If we assume (following the results of Sec. VI) that $V_{pd\pi} \approx -2.2S_\pi$, then the value of $(pd\pi)$ from Table II suggests that $S_\pi \approx -0.058$ and $V_{pd\pi} \approx 0.128$ Ry, which are quite reasonable values.

To illustrate the sensitivity of the parameters S_s, $(sd\sigma)$, and V_{sd} to the values assumed for the remaining parameters in Table II, we consider the results of Table VIII. Here, we compare selected energy eigenvalues for ReO_3 which are obtained via the methods of Sec. VI A as a function of the parameter

TABLE VIII. LCAO parameters and selected eigenvalues for ReO_3 as a function of E_s (in Ry).

	APW	LCAO	LCAO	LCAO
E_s	• • •	−1.3400	−1.3820	−1.4150
$(sd\sigma)$	• • •	−0.2849	−0.2802	−0.2729
V_{sd}	• • •	−0.2182	−0.1942	−0.1639
S_s	• • •	0.0988	0.1235	0.1528
State				
Γ_{12}	0.351	0.351	0.351	0.351
X_1	0.626	0.643	0.648	0.653
X_1	−0.532	−0.543	−0.548	−0.553
X_2	0.356	0.349	0.349	0.348
M_1	0.487	0.496	0.501	0.508
M_1	−0.480	−0.489	−0.494	−0.500

E_s. If E_s is lowered by 0.07 Ry, S_s increases by 50%, $(sd\sigma)$ is approximately unchanged, while V_{sd} decreases by 30%. Raising E_s provides a modest 0.01-Ry improvement in the accuracy of the energy eigenvalues. This suggests that it may be necessary to fit APW wave functions as well as energy eigenvalues in order to obtain a reasonably accurate representation of the band structure in terms of the LCAO interpolation scheme.

In concluding this section, we consider the application of these ideas to the sodium chloride and rutile structures. Many antiferromagnetic compounds possess these structures above their Néel points.[16] Let us consider the sodium chloride structure first.

For our purposes, the band-structure results of Ern and Switendick[24] for TiC, TiN, and TiO illustrate the necessary features. In all cases, we observe that the titanium $4s$-$4p$ bands are raised above the $3d$ bands by the same overlap-covalency effects which are responsible for the crystal-field splittings in the ReO_3 and perovskite structures. However, we note that the Γ_{12}-$\Gamma_{25'}$ splitting is relatively small compared to the e_g and t_{2g} bandwidths. This is due to the fact that both Γ_{12} and $\Gamma_{25'}$ are orthogonal to the ligand s and p orbitals in the sodium chloride structure. Consequently, the origin of this splitting in the sodium chloride structure is identical with that in the cubic transition metals, namely, nearest-neighbor d-d interactions.

The s, $p\sigma$, and $p\pi$ contributions to the crystal-field splittings are nonzero at other points in the Brillouin zone. By applying the LCAO method to the sodium chloride structure, one can show that the e_g bandwidth is proportional to $\Delta_s+\Delta_\sigma$ if the d-d interactions are negligible, where Δ_s and Δ_σ are given by Eq. (3.19). In the ReO_3 and perovskite structures, we have found that this bandwidth is proportional to $\Delta_\sigma-\Delta_s$. The t_{2g} bandwidth is proportional to Δ_π in all three structures, where Δ_π is given by Eq. (4.13). The fact that the e_g bandwidth in the NaCl structure is proportional to the sum $\Delta_s+\Delta_\sigma$ should lead to large values of b in Anderson's theory of superexchange. However this effect is compensated by the fact that the crystal-field and d-d interaction terms tend to cancel in this structure.

It is interesting to note that the crystal-field parameter in the localized Wannier limit Δ_{loc} which is given by Eq. (5.21) is also valid for the NaCl structure. Since we have already shown that this equation is equivalent to the results of MO theory, its validity depends only on the point symmetry of the metal-ligand octahedral complex, not on the manner in which these complexes are stacked together to form a three-dimensional crystal structure. Thus, in this localized limit, we have the interesting result that for a given octahedral metal-ligand complex, the magnitude of the crystal-field splitting is independent of the crystal structure, while the strength of the superexchange interaction J_{eff} should depend significantly on the details of the stacking arrangement.

The rutile structure presents a more challenging system for applying the LCAO method. As a matter of fact, the LCAO method was formulated in order to overcome difficulties which occurred in the application of the LCOAO method to this structure. The lower site symmetry of the transition-metal atom in the rutile structure removes the double and triple degeneracies of the octahedrally coordinated e_g and t_{2g} states. In applying the LCOAO method to fit preliminary APW results for RuO_2, it was found that this method required unrealistically large values for the d-d interaction parameters. We believe that the LCAO method will include these crystal-field effects in a more realistic manner and yield a more accurate and reliable fit to the APW results for these materials.

ACKNOWLEDGMENTS

I have benefited from several useful and informative discussions with Paul Soven and J. H. Condon during the entire course of this investigation. I also wish to acknowledge helpful conversations with C. Herring, P. W. Anderson, and W. F. Brinkman. Finally, I am indebted to J. E. Graebner and W. D. Ryden for providing their detailed experimental Fermi-surface data on several transition-metal oxides (particularly RuO_2) since it was the difficulties which were encountered in explaining their data in terms of the LCOAO model that inspired this study.

[1]L. F. Mattheiss, Phys. Rev. 181, 987 (1969).
[2]J. C. Slater and G. F. Koster, Phys. Rev. 94, 1498 (1954).
[3]S. M. Marcus, Phys. Letters 27A, 584 (1968).

[4]J. E. Graebner and E. S. Greiner, Phys. Rev. 185, 992 (1969).
[5]P. O. Löwdin, J. Chem. Phys. 18, 365 (1950).
[6]S. Sugano and R. G. Shulman, Phys. Rev. 130, 517 (1963).
[7]P. W. Anderson, in *Solid State Physics*, edited by F. Seitz and D. Turnbull (Academic, New York, 1963).
[8]See, for example, G. F. Koster, Technical Report No. 8, Solid-State and Molecular Theory Group, MIT, 1956 (unpublished); P. O. Löwdin, Research Report No. 213, Quantum Chemistry Group, Uppsala University, 1968 (unpublished).
[9]P. O. Löwdin, J. Chem. Phys. 19, 1396 (1951).
[10]R. E. Watson and A. J. Freeman, Phys. Rev. 134, A1526 (1964).
[11]E. Šimánek and Z. Šroubek, Phys. Status Solidi 4, 251 (1964).
[12]J. Owen and J. H. M. Thornley, in *Reports on Progress in Physics*, edited by A. C. Stickland (Stonebridge, Bristol, England, 1966).
[13]R. G. Shulman and S. Sugano, Phys. Rev. 130, 506 (1963).
[14]F. Herman and S. Skillman, *Atomic Structure Calculations* (Prentice-Hall, Englewood Cliffs, N. J., 1963).
[15]A. H. Kahn and A. J. Leyendecker, Phys. Rev. 135, A1321 (1964).
[16]J. S. Smart, in *Magnetism*, edited by G. T. Rado and H. Suhl (Academic, New York, 1963), Vol. III.
[17]J. C. Phillips, J. Phys. Chem. Solids 11, 226 (1959).
[18]K. Knox, R. G. Shulman, and S. Sugano, Phys. Rev. 130, 512 (1963).
[19]J. H. Wood, Phys. Rev. 117, 714 (1960).
[20]L. Pauling, *The Nature of the Chemical Bond*, 3rd ed. (Cornell U. P., Ithaca, N. Y., 1960).
[21]J. Waser, in *Structural Chemistry and Molecular Biology*, edited by A. Rich and N. Davidson (Freeman, San Francisco, 1968).
[22]M. Wolfsberg and L. Helmholz, J. Chem. Phys. 20, 837 (1952).
[23]C. Herring, in *Photoconductivity Conference*, edited by R. G. Breckinridge, B. R. Russell, and E. E. Hahn (Wiley, New York, 1956).
[24]V. Ern and A. C. Switendick, Phys. Rev. 137, A1927 (1965).

PHYSICAL REVIEW B VOLUME 2, NUMBER 10 15 NOVEMBER 1970

Determination of Long-Range Interaction Energies from the Scattering of X Rays by Disordered Alloys

Stephen Wilkins*
School of Physics, University of Melbourne, Parkville, Victoria 3052, *Australia*
(Received 20 November 1969)

A method for determining the interparticle interaction energies in a disordered alloy from the corrected diffuse scattering intensities of x rays is presented. This method, which is based on the ordering theories, is applied to the problem of obtaining the first seven pair-interaction ratios in Cu_3Au from the experimental data of Moss. Strong evidence for the presence of long-range pair interactions originating from the indirect screening interaction between ions is obtained for Cu_3Au, indicating the existence of a reasonably sharp Fermi surface in this alloy, at temperatures of the order of 700 °K.

I. INTRODUCTION

One of the principal objectives in experimentally investigating short-range order in a binary alloy is to obtain information on the magnitude, sign, and range of the interparticle interaction energies in such a system. The current state of alloy theory suggests that a realistic comparison between empirical and theoretical values for these interactions is possible.

Clapp and Moss,[1-3] in a recent series of papers (Ref. 3, in particular), obtained indications of the existence of an oscillatory interaction in the Cu-Au system by an indirect method requiring diffuse scattering data from alloys with different compositions. We present a method which indicates an oscillatory interaction through experimental results from a single alloy system.

The pair-interaction model[1-4] assumes the energy of the binary alloy AB, with atom fractions (m_A, m_B) to be decomposable into the sum of interactions V_{ij}^{AA}, V_{ij}^{BB}, V_{ij}^{AB}, and V_{ij}^{BA}, between pairs of atoms (A, B) at sites i and j and a term independent of configuration at constant volume. The pair-interaction energy parameter is usually defined as

$$V_{ij} = \tfrac{1}{2}(V_{ij}^{AA} + V_{ij}^{BB} - 2V_{ij}^{AB}) . \quad (1.1)$$

This model for calculating the energy of a binary alloy should improve in reliability as the size difference between the A- and B-type atoms decreases, when the contributions of irreducible n-body $(n > 2)$ strain-energy terms will likewise diminish.[2,5]

For zero-size-effect binary alloys of nontransi-